Contents

List of Figures

1.2 List of Tables

Chapter 1

1. Introduction

In this chapter, we shall give an overview of different cellulose fibers. Some background information on various cellulose allomorphs shall be reviewed. Structural properties of cellulose fibers shall be reported as well. Theoretical studies and some methods used shall be briefly introduced. Lastly, rationale, the objectives as well as outline of the dissertation are stated.

1.1 Background information

Cellulose is regarded as the most abundant polymer in nature, and the first on which X-ray investigation have been performed. The history on structural research of cellulose is illuminating since it shows the difficulties involved in solving crystal structures of polymers. Understanding the details of cellulose structure is increasingly important as the drive to use renewable resources in technological applications increases. Techniques that have probed cellulose structure have so far been of limited applicability in describing the cellulose surface, which is vitally important in many natural and industrial processes such as enzymic hydrolysis [1]. Today, the renaissance in the use of natural fibres as reinforcements materials in applications is taking place in automotive and packaging industries. There are at least four polymorphs of cellulose, namely cellulose Iβ, II, III, IV_1 and IV_2 [1-4]. The two most common polymorphs are cellulose I, the native form, and cellulose II, and the latter is the most stable polymorph.

The availability of large quantities of natural fibres with well-defined mechanical properties is a general prerequisite for the successful use of these materials and

lack of these properties is one of the drawbacks at the present moment. Despite its importance in industrial applications, relatively little is known about detailed structure at mesoscopic level. Refinements carried out both with P_{21} and P_1 symmetry indicate that cellulose Iβ and II structures are both reasonably well described by P_{21} symmetry [5].

Short conventional fiber (glass, aramid, carbon, etc) has been extensively used over the last decades as reinforcements of thermoplastic polymeric matrices. They are incorporated into plastics with the main objective of improving the mechanical properties of the polymer reducing the cost of the final products [6-8] with respect to long fibre composites. It has been known for years that the loss of mechanical properties of cellulose due to durable press treatments can be severe, thus, cellulose, as with other polymers, is limited in its morphology [9].

The reasons why there is renewed interest in cellulose fibres are as follows: Over the last twenty years there has been a large investment in technology to reduce the amount of chemicals which cause pollution and recover and re-use them. Cellulose is a renewable resource, unlike oil or wool, which synthetic fibres depend on. Cellulose is one of the oldest natural polymers and also renewable, biodegradable, and can be derivatized to yield useful products. Several disadvantages of cellulose include its expensive production, its sensibility to water, and its slow regeneration- a tree must have at least 30 years before it can be used for cellulose production [10]. In most cases, the substitution of glass fibers by natural fibers is precluded first of all by economic reasons. But natural fibers offer several advantages over glass fibers. Plant fibers are renewable raw materials and their availability is more or less unlimited. When natural reinforced plastics were subjected, at the end of their life cycle, to a combustion process or landfill, the amount of carbon dioxide from fibres is released with respect to the assimilated amount during the growth.

1.2 Basic information on cellulose structures

Cellulose is a complex carbohydrate, $(C_6H_{10}O_5)_n$, which is composed of glucose units. It is a polymer, or more specifically a polysaccharide, which is made of more than 3,000 glucose units. It forms the main constituent of the cell wall in most plants, and is important in the manufacture of numerous products, such as paper, textiles, pharmaceuticals, and explosives.

1.3 The chemistry of cellulose

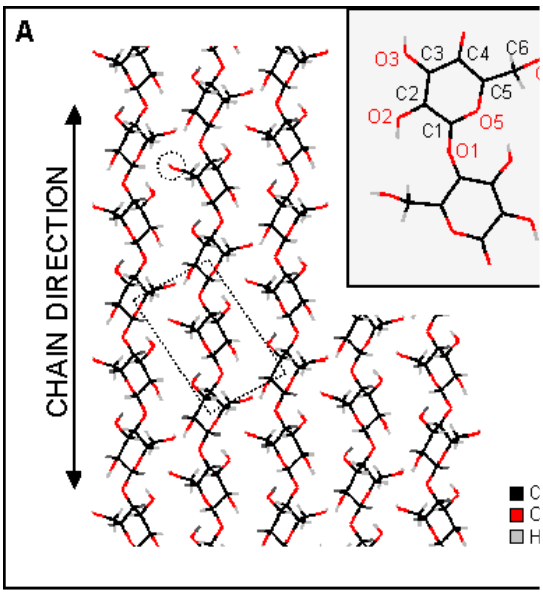

Figure 1.Cellulose chains with monomer atomic numbering [11]

Eliminating the water between monosaccharide molecules produces polysaccharide, like cellulose. It accounts for more than half of all living matter, and is the basic structural component of plant cell walls. Cellulose makes up 99% of cotton and 55% of wood and is the most abundant natural, organic compound in the world [11]

Although the melting and boiling point of cellulose are not defined, the decomposition temperature is 260-70 ^{o}C, the density in natural state is between 1.27 to 1.60 g/ml. The chemical formula of a monomer and its molar mass are $C_6H_{10}O_5$ and 162.0 g. 44.4% weight of cellulose is carbon; 6.2% weight is hydrogen and 49.4% weight is oxygen [11]. In the cellulose chain, the glucose units are in 6-membered rings, called pyranoses. They are joined by single oxygen atoms (acetal linkages) between the C-1 of one pyranose ring and the C-4 of the next ring. Since a molecule of water is lost when an alcohol and a hemiacetal react to form an acetal, the glucose units in the cellulose polymer are referred to as anhydroglucose units.

The spatial arrangement, or stereochemistry, of these acetal linkages is very important. The pyranose rings of the cellulose molecule have all of the groups larger than hydrogen sticking out from the periphery of the rings (equitorial positions). The stereochemistry at carbons 2, 3, 4 and 5 of the glucose molecule are fixed; but when glucose forms a pyranose ring, the hydroxyl at C-4 can approach the carbonyl at C-1 from either side, resulting in two different stereochemistries at C-1. When the hydroxyl group at C-1 is on the same side of the ring as the C-6 carbon, it is said to be in α configuration (not to be confused with α - cellulose, which is not related). In cellulose, the C-1 oxygen is in the opposite, or β configuration (*i.e.*, cellulose is poly [β -1, 4-D-anhydroglucopyranose]. This β configuration, with all functional groups in equatorial positions, causes the molecular chain of cellulose to extend in a more-or-less straight line, making it a good fiber-forming polymer. Amylose, a constituent of starch, is a related polymer of glucose, but with the C-1 oxygens in α configuration. This configuration forces the linkage to the next glucopyranose ring to assume an axial position, and the starch molecules tend to coil, rather than extend. Even though it often has long molecular chains, amylose is not a good fiber-former.

Owing to the equatorial positions of the hydroxyls on the cellulose chain, they protrude laterally along the extended molecule. This positioning makes them readily available for hydrogen bonding. These hydrogen bonds cause the chains to group together in highly ordered (crystal-like) structures. Since the chains are usually longer than the crystalline regions, they are thought to pass through several different crystalline regions, with areas of disorder in between (the "fringed-micelle" model) [11]. The inter-chain hydrogen bonds in the crystalline regions are strong, giving the resultant fibers good strength and insolubility in most solvents. They also prevent cellulose from melting (*i.e.*, non-thermoplastic). In the less ordered regions, the chains are further apart and more available for hydrogen bonding to other molecules, such as water. Most cellulose structures can absorb large quantities of water (*i.e.*, it is very hygroscopic). Thus, cellulose swells, but does not dissolve in water [12].

1.4 Structural aspects

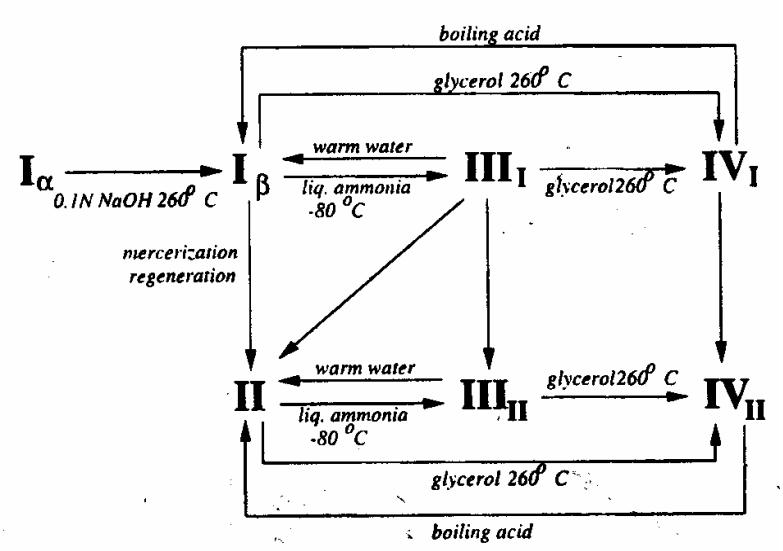

Figure 2 Polymorphy of cellulose and the reactions involved [11]

Native crystalline cellulose, commonly known as cellulose I, gives rise to at least three polymorphic structures upon appropriate treatment [13], whose links are depicted in figure 2. The regeneration or mercerization results in cellulose II and both the latter as well as cellulose I can be converted to cellulose III through the use of liquid ammonia. Cellulose III in turn, can be converted to cellulose IV by heat treatment. All four polymorphs crystallize well and their structures apparently differ only in the crystalline packing of chains with nearly the same conformation, because all four polymorphs show the same fiber repeat of ~10.3 Angstroms. The highly crystalline cellulose I of alga Vanolia ventricosa has been previously shown to crystallize with parallel packing of chains [14, 15]. Whether the same is true for the less crystalline native celluloses of ramie, cotton, etc., is presently not known, but their X-ray diffraction patterns are nearly identical with that of Valonia, although less well resolved. Conversion of ramie or cotton cellulose II results in a structure that is based on antiparallel packing of chains [16, 17].

1.4.1 Cellulose Iβ

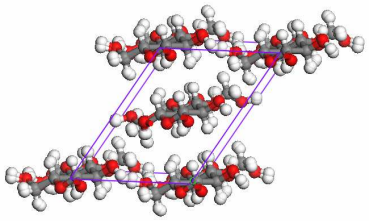

Figure 3(a) The structure of cellulose Iβ. Red is oxygen; white hydrogen and grey carbon.

There are two allomorphs of cellulose I; cellulose Iα, predominates in algal celluloses [18,19] and cellulose Iβ, mostly found in plant celluloses. Cellulose Iβ is more stable than cellulose Iα [20, 21 and 22]. The structure of cellulose Iβ is

given in figure 3a and the corresponding fractional coordinates are reflected in table A of Appendix B, and have been obtained from Zugenmaier [22]. A recent overview on Valonia [23] cellulose summarizes the structure of various results of the determination of cellulose Iβ (algal, ramie etc.). The excepted structure of the Iβ allomorph has been proposed in the monoclinic space group P_{21} by Gardner and Blackwell [24], and Sarko and Muggli [25] using fiber diffraction methods. Cellulose Iβ is monoclinic and has fiber repeat unit of 10.3Å, which is common to all polymorphs.

1.4.2 Cellulose II

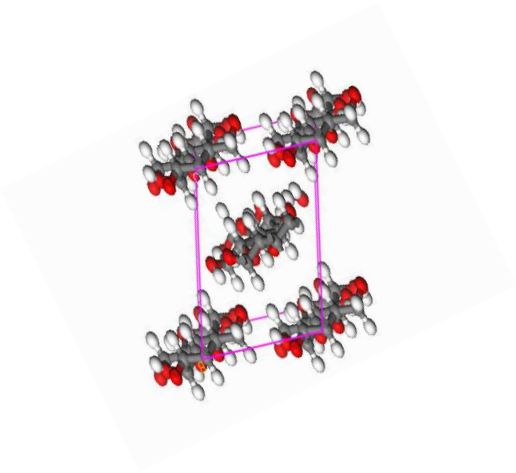

Figure 3b Structure of cellulose II.

The structure of cellulose II is shown in figure 3b and the corresponding fractional coordinates are given in table B of Appendix B. Mercerization by intracrystalline swelling of native cellulose in NAOH and washing and drying leads to cellulose II as well as regeneration by spinning out of solution. Both procedures lead to almost identical unit cells. The refinements strategy for cellulose II follows that of Cellulose I by evaluation of X-ray data and potential energy calculation. In

contrast to cellulose I, antiparallel chains of regenerated cellulose previously proposed by Kolpak and Black well [26] or as suggested by Sarko and Muggli [27] some years earlier have been confirmed in recent investigations based on the structural data of model compounds and additional neutron diffraction data [28]. Intramolecular hydrogen bonding for both origin and center chains occur between O_3 and adjacent O_5 of the next residue. Intermolecular hydrogen bonds occur in the intersheets to form an optimal hydrogen bonding network in contrast to cellulose Iβ where only intrasheets hydrogen bonds have been detected and a slipping of sheets appears possible.

1.4.3 Cellulose III

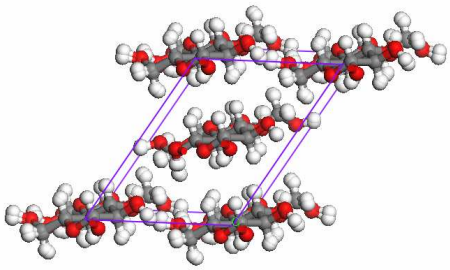

Figure 4 (a) The structure of cellulose III

The basic unit cell of cellulose III is given in figure 4a and the corresponding fractional coordinates of the structure are reflected in table C of Appendix B. The two structures cellulose III_1 and III_2 can be prepared by the same treatment with liquid ammonia, only the starting material being different, which may be for cellulose III_1 native ramie, cotton or hemp and for cellulose III_2 mercerized ramie, Fortisan rayon [29]. The unit cell for both crystalline structures is the same, but especially the meridional reflections differ. However, the two structures pack in quite a different fashion [30], parallel arrangements in III_1 and antiparallel in III_2 concluded from the fact that cellulose III_1 can be converted by mild heat treatment

to parallel packed cellulose I and cellulose III_2 by the same treatment to antiparallel cellulose II. It is close to I and II in conformation and hydrogen bonding. Cellulose III_1 has the same conformation and hydrogen bonding scheme as cellulose I along chains and only intrasheets ones between various chains. The difference between I and III_1 is a shift in intrasheets against each other. Ribbon like cellulose chains are slightly tilted out of the intrasheet planes allowing a contraction of the **b** dimension and forcing **a** to widen.

When, for example, ramie cellulose I or cellulose II is treated with liquid ammonia, two different cellulose III diffraction diagrams are obtained: the so-called III_1 from cellulose I and the III_2 from cellulose II [31]. Both are nearly, but not completely, identical. Mild treatment, such as heating in water, reverts cellulose III_1 back to Cellulose I and cellulose III_2 back to cellulose II.

1.4.4 Cellulose IV

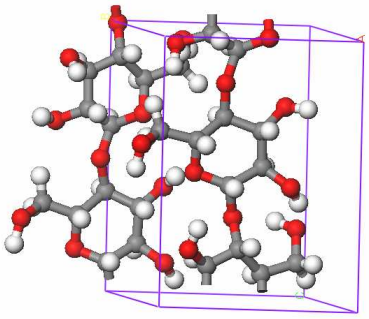

(b)

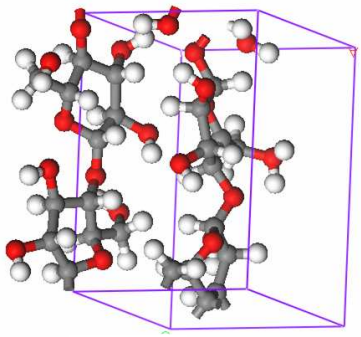

(c)

Figures 4 (b) and (c) Strcutrues of cellulose IV_1 and $1V_2$ respectively

Structures of cellulose IV_1 and $1V_2$ are shown in figures 4 b and c and their corresponding fractional coordinates are given in table E of Appendix B. Cellulose IV is produced from cellulose III sources mentioned above by heating in glycerol

at 260 °C for 20 min [29] and, as expected, two structures are formed and denoted correspondingly to the starting materials as cellulose IV_1 and IV_2. The poor diffraction diagrams and their unit cells are very similar, but their derived structures can be distinguished upon heterogeneous acetylation, since cellulose IV_1 reversibly transforms to parallel packed cellulose triacetate I and cellulose IV_2 to antiparallel packed cellulose triacetate II [32]. The size of the unit cell for cellulose IV_1 resembles very much that of cellulose Iβ with an angle $\gamma = 90°$ instead of 96.3°. P_1 space group is assumed to be as a consequence of packing consideration. Unit cell parameter a, equals almost b within experimental error and $\alpha=\beta=\gamma=90°$. In classifying cellulose allomorphs, it can be stated that cellulose crystal structures fall into two families that differ in chain polarity: the parallel chain family (cellulose Iα, Iβ, III_1 and IV_2) and the antiparallel-chain family (cellulose II and IV_2).

1.4.5 Bonding within the cellulose structure

Studies of cellulose degradation by Nam. et al [33] highlighted the presence of two types of hydrogen bonds in cellulose molecules: those that form between C-3 and OH group and the oxygen in the pyranose ring within the same molecule and those that form between C-6 and OH group of one molecule and the oxygen of the glucosidic bond of another molecule. Ordinarily, the beta-1,4 glycosidic bonds themselves are not too difficult to break. However, because of these hydrogen bonds, cellulose can form very tightly packed crystallites. These crystals are sometimes so tight that neither water nor enzymes can penetrate them; only exogluconase, a subgroup of cellulase that attacks the terminal glucosidic bond, is effective in degrading it. The inability of water to penetrate cellulose also explains why crystalline cellulose is insoluble. On the other hand, amorphous cellulose allows the penetration of endogluconase, another subgroup of cellulase that catalyzes the hydrolysis of internal bonds. The natural consequence of this

difference in the crystalline structure is that the hydrolysis rate is much faster for amorphous cellulose than crystalline cellulose.

Cellulose	Number of atoms	Density g/cm^3
Iβ	84	1.60793
II	84	1.60430
III	116	1.89091
IV_1	84	1.60165
IV_2	84	1.60009

Table 1. Crystal structure densities and number of atoms of celluloses studied

The process of breaking the glucosidic bonds that hold the glucose basic units together to form a large cellulose molecule is called hydrolysis because a water molecule must be supplied to render each broken bond inactive.

1.5 Physical properties of cellulose

Although cellulose produced by different organisms have the same chemical composition, polymer of β-1, 4-linked glucose residues, there are remarkable differences in the physical properties of the cellulose products, mainly in the chains of the glucan chains (as represented by degree of polymerization) and the crystallinity and crystalline form of the cellulose product. Depending upon the specific organism, this crystalline state is different, and it defines the physical properties of the product such as its strength, solubility in various solvents, and accessibility to various modifying agents [34].

The variability in the properties of wood and wood fibers is of importance for the ability to use the material in the wood industry as well as for manufacturing paper products. For example, the elastic moduli of wood fibers are important for the pulp and paper making processes as they influence the flexibility and conformability of the fibers, and thus the ability of the fibers to conform and bond to each other. To a large extent, fiber bonding determines the strength properties of the paper sheet. Cellulose is one of the three major polymers, the other two being; hemicellulose and lignin, all of which are arranged into a natural fiber-reinforced composite. Apart from these, smaller contents of pectin and proteins also exist in some parts of the cell wall, giving strength and stiffness to the tree. Lignin acts as a supportive material to the cellulose, preventing the cellulose micrifibril from buckling under compression [35].

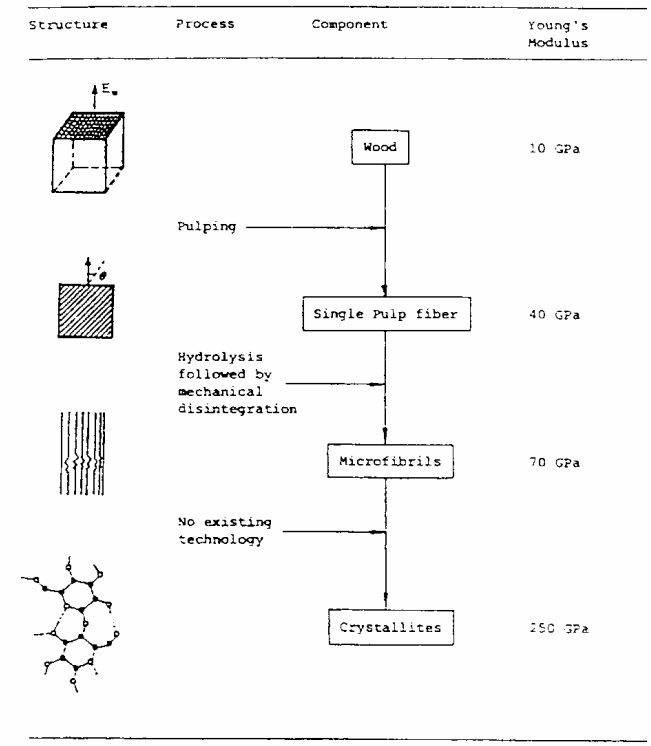

Figure 5. Young's modulus and structure of cellulose [35]

Hemicelluloses are branched heterosaccharides built up of two to six different monosaccharides. Lignin is a there-dimensional natural polymer consisting of three phenyl propane monomers or monolignols [35]. Pectin is a collective name for heteropolysaccharides, which consists essentially of polygalacturon acid. Pectin is soluble in water only after a partial neutralization with alkali or ammonium hydroxide [36, 37]. Figure 5 shows the correlation between the structure, processes, the resulting component as well as the respective Young's moduli of various structures.

Natural fibers may be broadly classified into two types, carbohydrates (for example, the cellulose-based cotton and flax) and proteinaneous (for example, the Keratotic animal furs generically termed wool and the insect-based secretions termed silk). Current knowledge about the crystal structure of native cellulose, so-called cellulose I, is still in flux. Although a crystal structure has been proposed [38,39] on the basis of X-ray and electron diffraction data as well as chain packing energetics, others [40,41] would argue against the claim that aside from differing degree of disorder, all native celluloses have the same crystal structure. The question of parallel and antiparallel is still discussed. Differences such as the relative rotation of neighbouring chains about the respective chain axes and the conformation of the primary alcohol group are admittedly known with less precision. The technology for the use of natural fibres as reinforcing fillers has fallen significantly behind that of more conventional fibres such as glass and carbon fibres. In order to optimise the mechanical performance of these composites, it is necessary to understand microstructure-property relationships [42]. More than 60 years have passed since the general features of native crystalline cellulose were outlined by Meyer and Mark [43,44]. Since the work of these pioneers, the resolution of three-dimensional structure of crystalline cellulose has been the focus of a number of investigations [45,46].

Even though cellulose has been one of the most studied polymers, its crystalline structure remains only partially understood. At any rate, Vanolia cellulose I is the widely accepted native cellulose standard, having the highest crystallinity and perfection [47]. Since the early 1960s, there has been an ever-increasing demand for newer, stronger, stiffer, and yet lightweight materials in fields such as aerospace, transportation and construction. High demands on materials for better overall performance had led to the extensive research and development efforts in the composites fields. These materials have low specific gravity that makes their properties particularly superior in strength and modulus to many traditional engineering materials such as metals. Today, five major classes of composites materials exist: ceramic matrix composites (CMC), metal matrix composites (MMC), intermetallic matrix composites (IMC), carbon-carbon composites (CCC) and polymer matrix composites (PMC)

1.6 Computational modelling techniques

The use of computational modelling in studies of cellulose structure can be traced back to the early 1980s [48]. Since then, its has been helpful in interpreting X-ray diffraction data for cellulose crystals and to aid in understanding the structures of cellulose I and II [48, 49]. While computers have increased the range of systems which are possible to study, the techniques available have also grown tremendously. This means that the calculations, which were not possible few years ago, are now trivial to perform. Despite these developments, computational techniques such as energy minimization, molecular dynamics, molecular mechanics, Monte Carlo and electronic structure techniques are used to fill the information gap between fundamental materials-science and industrial applications. Computational techniques can help to understand and design complex materials

and offer an attractive approach in many fields where experimental data is rare and difficult to obtain. As a result, using the computational methods, alone or in combination with experiments, it is possible to model and predict structures, characterize bonding in solids, model surfaces and interfaces, atomic transport and defect structures, chemical reactions, phase transformations, docking or predict reaction mechanisms [49]

1.7 Objectives and Outline of the dissertation

1.7.1. Objectives

We will confine our study to the following aspects:

Numerous authors used various techniques and systems of different origins to study properties of cellulose. In this work, computational modelling studies will be extensively utilized to study structural and mechanical properties of cellulose. Classical simulation methods, involving energy minimization and molecular dynamics (MD) technique will be employed to computationally simulate crystalline structures of cellulose. We shall determine mechanical properties i.e. bulk modulus, tensile strength, shear modulus etc. of the bulk systems. Molecular dynamics will be used to determine the structures of bulk cellulose at different temperatures from the radial distribution functions (rdf's). Also lattice parameters, which give information about the volume of the system, will be determined at different temperatures; however, there is no experimental work available thus far. Furthermore, our work will involve subjecting our material to various temperatures and pressures and the effect shall be monitored. The effect of water on both structural and mechanical properties will be of interest in the study. We will, where data is available, compare our results with what has been reported in the literature and elsewhere.

1.7.2 Outline of the dissertation

The dissertation is partitioned into four chapters outlined as follows:

Chapter one gives some basic information, theory and background on cellulose fibers, some work which was previously done. Structural aspects, rationale, and objectives are also outlined.

Chapter two reports on the methods, which were employed in the study; energy minimization and molecular dynamics (MD) techniques, force field (Compass and PCFF) as well as the code used, DISCOVER.

Chapter three gives, in full, the report on the results obtained as well as some discussions emanating from our calculations. These include results on structural and mechanical properties of systems under investigation. Some related work done previously is highlighted.

Chapter four presents conclusion and recommendations drawn from the study based on the results obtained. Finally, the appendix and the bibliography are also listed

Chapter 2

2 Methodology

2.1 Introduction

Theoretical techniques allow both interpretation of experimental data and prediction of new material properties. Computational modelling methods allow us to directly correlate atomic structural models with experiment. Extensive computational modelling can complement and sometimes even replace traditional methods of trial and error experimentation.

This chapter is mainly concerning the computational approaches employed and calculations carried out in the study. There are a number of theoretical methodologies that are known and used in Materials Science. These include Ab Initio, Molecular Mechanics (MM), Monte Carlo (MC) and these are used to fill the informational gap between materials science research and industrial applications.

Firstly, the minimum energy structures were obtained using the energy minimization technique. Energy minimization takes no account of the temperatures, but a structure whose energy has been minimised serves as a good starting material for a desired calculation. Some theoretical background on the method used is broadly stated in this chapter. Prediction of material properties make use of two approaches; the force field or empirical potential methods that avoids details of electronic structure and consider the interactions of atoms in a quasi-classical form. In this work we have based our calculations on the force field or empirical potential methods. Molecular dynamics simulation technique was

extensively employed in the simulation program; DISCOVER code, in conjunction with both the PCFF and Compass force fields [50]

2.2 Classical simulations theory

Accurate simulation of atomic and molecular systems generally involves the application of quantum mechanical theory. However, quantum mechanical techniques are applied to small systems or small molecules. It is not practical to model large systems such as a condensed polymer containing many thousands of monomers in this way. Even if such a simulation were possible, in many cases much of the information generated would be discarded. This is because in simulating large systems, the goal is often to extract bulk (statistical) properties, such as diffusion coefficients or Young's moduli, which depend on the location of the atomic nuclei or, more often, an average over a set of atomic nuclei configurations. Under these circumstances the details of electronic motion are lost in the averaging processes, so bulk properties can be extracted if a good approximation of the potential in which atomic nuclei move is available and if there are methods that can generate a set of system configurations which, while they may not follow the exact dynamics of the nuclei, are statistically consistent with a full quantum mechanical description.

There are a number of potentials (or force fields) and distribution generating techniques available and they are collectively referred to as classical simulation methods. The term classical is used because some of the earliest simulations generated configurations by integrating the Newtonian (Classical) equations of motion and this approach is still widely used. The material in this section gives a general overview of the principal elements of classical simulation, while the detailed implementation of these techniques used by Discover and Forcite are documented separately.

2.3 Simulation methods

The approach taken by Computational Materials Scientists is formulation of a set of integrated predictive models that bridge the time and length scales associated with material behavior from the nano through to meso scale. At the atomistic or molecular level, the reliance is on molecular mechanics, molecular dynamics, and coarse grain, Monte Carlo simulation. Molecular models encompassing thousands and perhaps millions of atoms can be solved by these methods and used to predict fundamental, molecular level material behavior. The methods are both static and dynamic. For example, molecular mechanics can establish the minimum-energy structure statically and molecular dynamics can resolve the nanosecond- scale evolution of a molecule or molecular assembly. These approach can model both the bonded and non bonded forces (e.g., Van der Waals and electrostatic, but cannot exclusively account for bond cleavage.

2.4 Energy minimization technique.

In molecular modelling, the interest is especially in minimum points on the energy surface. Minimum energy arrangements of the atoms correspond to stable states of the system; any movement away from a minimum gives a configuration with a higher energy. There may be very large number of minima on the energy surface. The minimum with the lowest energy is known as the global energy minimum. A minimization algorithm is used to identify those geometries of the system that correspond to the minimum points of the energy surface. The highest point on the pathway between minima is of special interest and is known as the saddle point with the arrangement of atoms being the transition structure.

In order for the aforementioned potential model to be useful in predicting perfect lattice properties, it must be combined with an energy minimization technique to bring the system to a state of mechanical equilibrium. All atomic interactions are

calculated and each atom subsequently moves a distance proportional to the force acting on the particle in the direction of the overall field. There are two approaches that are in common use for minimising the lattice energy, either at constant volume or constant pressure. During constant volume minimization, the cell dimensions are fixed but the atoms are allowed to move in space. This means that no consideration is made of the bulk lattice strain. For constant pressure techniques, it is necessary to determine the minimum energy not only through adjustment of atomic coordinates, but also unit cell dimensions, accounting for the strains both on individual atoms as well as the unit cell. Thus, in case of constant pressure minimization both cell dimensions and atomic coordinates are allowed to change.

Bad Van der Waals contacts, highly distorted bonds or angles can be built in the structures. Minimization is used to relax those areas at which very strong interactions would occur. After that, dynamics can start with a reasonable structure with no exceedingly strong forces. If MD is started with an unsuitable structure, the strong forces between unsuitable contacts would cause the structure to move a great deal during a short time step, causing the structure to collapse or fly apart. The potential energy calculated by summing the energies of various interactions is a numerical value for a single conformation. This number can be used to evaluate a particular conformation, but it may not be a useful measure of conformation because it can be dominated by a few bad interactions. For instance, large molecule with an excellent conformation for nearly all atoms can have a large overall energy because of a single unsuitable interaction, for instance two atoms too near to each other in space and having a huge van der Waals repulsion energy. Thus, it is often preferable to carry out energy minimization to find the best nearby conformation. Energy minimization is usually performed by gradient optimisation: Atoms are moved so as to reduce the net forces on them. The minimized structure has small forces on each atom and therefore serves as an excellent starting point of

molecular dynamics simulations. The problem with energy minimisation calculations is that they take no account of temperature.

2.5 Classical molecular dynamics simulation method

2.5.1 Background and theory

Molecular dynamics simulation is a computer simulation technique where the time evolution of a set of atoms is followed by integrating their equations of motion. Molecular dynamics (MD) calculates ‘real’ dynamics of the system from which time averages of properties can be calculated. The major disadvantages however, is that it is time consuming and can be computationally expensive. To a large extent this has been offset with the development of more efficient simulation packages and advancement of computer technology. This makes it possible to undertake molecular dynamics simulation on a desktop PC.The molecular dynamics (MD) method was first introduced by Alder and Wainwright in the late 1950's to study the interaction of spheres [51, 52]. The next major advance was in 1964, when Rahman carried out the first simulation by using a realistic potential for liquid argon [21]. A molecular dynamics simulation of organic and inorganic material systems addresses a variety of issues including the thermodynamics of biological process, polymer chemistry and crystal structure [53, 54]. Molecular dynamics simulation techniques are widely used to help interpret experimental results from X-ray crystallography and nuclear magnetic resonance spectroscopy. MD simulations generate information on the nano level, including atomic positions and velocities. In Molecular dynamics simulation, the time dependent behavior of the molecular system is obtained by integrating Newton's equations of motion. The result of the simulation is a time series of conformations or the path followed by each atom. Most molecular dynamics simulations are performed under conditions of constant number of atoms, volume, and energy (N, V, E), or

constant number of atoms, temperature and pressure (N, T, P) to better simulate experimental conditions.

In MD, atoms interact with each other, the forces acting upon the atoms are caused by the interactions between atoms and the atoms move under the action of the instantaneous forces. As the atoms are moving, their relative positions and forces change. Sets of atomic positions are derived in sequence by applying Newton's equations of motion. MD is a deterministic method, thus, the state of the system at any future time can be predicted from its current state. In MD, laws of classical mechanics are followed and notably Newton's law for each atom i in the system constituted by N atoms. Many different fields, from materials science to pharmaceuticals make use of MD simulation technique extensively. Some background information about MD is obtained by referring to [55-57]. MD technique is used to simulate the movements of particles in a system over time. Each of the particles i in the system has an initial position $\acute{r}_i$ (t_0) and an initial velocity v_i (t_0) at time $t = t_0$. Given the number of particles in the system, the initial temperature, the initial density, and the volume of the system, the MD simulation determines the trajectory of the system from $t = t_0$ to some later time $t = t_f$. The trajectory is basically the positions of the particles in the system as time advances. The simulation also keeps track of properties of the system such as total energy, potential energy, and kinetic energy. In order to compute the system's trajectory, the positions of all the molecules at time $(t + \Delta t)$ are calculated based on the positions of the particles of all the molecules at time t, where Δt is a small time interval. There are many methods for calculating the new positions; the most popular is the velocity Verlet algorithm. The steps in the algorithm are the following:

- calculate the velocity of each molecule at time $(t + \Delta t/2)$ based on the acceleration of each molecule at time t.
- using the newly calculated velocities, calculate the molecular positions at

$(t + \Delta t)$

- based on the new positions, calculate accelerations a_i $(t + \Delta t)$
- based on the newly calculated accelerations, calculate the velocities at time $(t + \Delta t)$.

The usefulness of a computer simulation largely depends on its quality. The most important factors that limit the accuracy of simulated results are discussed. The accuracy of different simulation studies differs by orders of magnitude. The accuracy will depend on the type of molecular system and process studied. It will also depend on the choices of force filed, the simulation set-up and the protocol that is used.

While minimization computes the forces on the atoms and changes their positions to minimize the interaction energies, dynamics computes forces and moves atoms in response to the forces. Molecular dynamics solves the classical equations of motion for a system of N atoms interacting according to a potential energy force field. Dynamics simulations are useful in studies of the time evolution of a variety of systems at nonzero temperatures, for example, biological molecules, polymers, or catalytic materials, in a variety of states, for example, crystals, aqueous solutions, or in the gas phase. To study the behavior of a solid, liquid or gas, a computer can be used to calculate the motions of all the individual molecules as they evolve with time. This approach is called "molecular dynamics" simulation. The molecular dynamics simulation technique was developed to simulate the time evolution of molecular systems. More information about a system can be obtained from molecular dynamics simulations. In these calculations, calculating the forces from the force field and, from this, the accelerations and velocities, follows the motions of particles. There are several ways in which this can be used. The normal ordinary molecular dynamics is the one in which the system or molecule is first energy-minimized, which optimises the structure of the system, then slowly heated and equilibrated through a preliminary simulation and then allowed to evolve at a

constant model temperature for a period of time sufficient to exhibit the behaviour of interest. Three traditional ways in which MD has been used are, Conformational Searching that involves the introduction of thermal energy into the system, Simulated Annealing, which is a means of removing residual strains in a structure by allowing it to "melt" or become more fluid internally, then cooling it back to it's starting temperature. Lastly, the Quenched Dynamics, which entails a rapid, drop in temperature to freeze the system. In the broadest sense, molecular dynamics is concerned with molecular motion. Motion is inherent to all chemical processes. Newton's equation is used in the molecular dynamics formalism to simulate atomic motion:

$$Force = mass \times acceleration (F = m_i a_i) \qquad (5)$$

The Leap-Frog algorithm [58] is an integration algorithm, where velocities are incorporated. It is essentially equal to the Verlet [58, 59] algorithm, and is given by equation (7) and (8). The "Leap-Frog" method is a common numerical approach to calculating trajectories based on Newton's equation. The steps can be summarized as follows: Solve for a_i at t using

$$-\frac{d\mathrm{E}}{dr_i} = F_i = m_i a_i(t) \qquad (6)$$

Update v_i at $t+\Delta t/2$ using:

$$\nu_i(t + \Delta t/2) = \nu_i(t - \Delta t/2) + a_i(t)\Delta t \qquad (7)$$

Update r_i at $t+\Delta t$ using:

$$r_i(t + \Delta t) = r_i(t) + v_i(t + \Delta t/2)\Delta t \quad (8)$$

The method derives its name from the fact that the velocity and position information successively alternate at 1/2 time step intervals

The MD technique is used to solve the equations of motion for a system of N-molecules interacting via a potential V, where V is given by: -

$$V(r) = \sum_i V(r_i) + \sum_i \sum_{j>i} V(r_i, r_j) + \sum_i \sum_j \sum_{k>j>i} V(r_i, r_j, r_k + \ldots$$
$$+ \sum_i \sum_j \sum_k)\ldots \sum_N V(r_i, r_j, r_k, \ldots, r_N) \quad (9)$$

which depends on coordinates of the individual atoms, pairs or triplets.

Consider the Lagrangian equation of motion, which is given by: -

$$\frac{d}{dt}\left\{\frac{\partial L}{\partial r_k}\right\} - \left\{\frac{\partial L}{\partial r_k}\right\} = 0 \quad (10)$$

in cartesian coordinates, r, over all atoms where L (r', r) is the Lagrangian function defined in terms of kinetic and potential energies.

$$L = K - V \quad (11)$$

where

$$K = \sum_i^N \tfrac{1}{2} mr \quad (12)$$

and

$$V = \sum_{i}^{N} \sum_{j>i}^{N} \nu\,(r_{ij}) \qquad (13)$$

$$L = \sum_{i}^{N} \frac{1}{2} m r_i^{\,2} + \sum_{i}^{N-1} \sum_{j>i}^{N} \nu(r_{ij}) \qquad (14)$$

where m is the mass of the N- atoms and the potential energy is assumed to be pair-wise additive of the individual potential between two atoms and is a function of the inter-atomic separation r_{ij}

Substituting L or equation (6) in equation of motion (3) gives the Newtonian formulation, force F, which is equal to mass, multiplied by acceleration.

$$ma = -\Delta r_i \{ \sum_{j=i} \nu\,(r_{ij}) \} \qquad (15)$$

This leads to a total of 3N second order differential equations or equivalently 6N first order equations. There are several conserved variables during the motion, on assuming that kinetic and potential energies do not depend explicitly on time, and that the form of the equations of motion guarantees that the total derivatives of the Hamiltonian, H,

$$\frac{\partial H}{\partial t} = 0 \qquad (16)$$

hence the Hamiltonian is constant of the motion, which is the conservation law, which applies whether or not an external potential exists. The essential condition is that no explicit time-dependent (or velocity-dependent) forces will act on the system. The second point concerning the equation of motion is that they are

reversible in time, by changing the sign of the velocities or the momenta of molecules; this enables one to trace their trajectories.

The potential energies V describe the Born-Oppenheimer surface of the atom's motion. Since it is difficult to obtain the surface quantum chemically by solving Schrödinger equation of a system for every atom configuration and for larger polymer systems, an empirical representation called Force field is used. A typical force field consists of terms accounting for two body interactions (covalent bonds and nonbonded interactions), van der Waals and electrostatic interactions, three body angle vibrations and the four body dihedral motions. A representation of the force field is given by:

$$V(r) = \sum_{Bonds} k_d / 2(d - d_0) + \sum_{Bondangles} k_\theta(\theta - \theta_0) + \sum_{\mathrm{Im}\, properdihedrals} k_b / 2(b - b_0)$$
$$+ \sum_{Dihedralangles} k_y / 2[1 - \cos(n\{y - y_0\})] + \sum_{Nonbondedpairs} 4\mathrm{E}_{ij}[(\sigma_{ij} / r_{ij})^{12} - (\sigma_{ij} / r_{ij})^{6}]$$
$$+ 1/4\pi\mathrm{EE}_0(q_i q_j / r_{ij}) \qquad (17)$$

where are force constants, d, θ, y, b are bond length, bond angles, dihedral angle and harmonic dihedral respectively, whereas d_0, θ_0, y_0, b_0 and θ_0 are their equilibrium values.

n = periodicity of the torsional potential.

r_{ij} = distance between two nonbonded atoms i and j

q_i and q_j = are the charges on the atoms i and j

E_{ij} = well depth

σ_{ij} = contact radius of the Lennard-Jones potential between the atoms i and j

E_0 = vacuum permittivity, 8.854 x $10^{-12}C^2J^{-1}m^{-1}$.

E = effective dielectric constant of the medium.

The Lennard-Jones parameters for pairs of unlike atoms are often calculated from the single parameters E_i, E_j, σ_i, σ_j by the use of mixing rules.

As an example the Lorentz-Berthelot mixing rules is given by:-

$$E_{ij} = \sqrt{(E_{ii}.E_{jj})}/2 \qquad (18)$$

and

$$\sigma_{ij} = (\sigma_{ii} + \sigma_{jj})/2 \qquad (19)$$

Nonbonded interacting by a bond or bond angles term (first and second neighbors) and they are often modified for the end atom of a dihedral angle.

The term r^{-12} and r^{-6} in equation (17) describes the interatomic repulsion and an attractive dispersive interaction respectively. Some force fields have cross terms between different degrees of freedom.

2.6 Total energy and force fields

2.6.1 The purpose of force fields

The development of force field, as a fundamental issue underlying all atomistic simulations, has drawn considerable attention in recent years, marked by publications of several revised or newly developed general force fields in the last 10 years. Among many of them, MM3, MM4, Dreiding,,SHARP, VALBON, UFF,CFF,AMBER,CHARM,OPLS,MMFF, COMPASS and PCFF. However, in this study, PCFF and Compass force fields were used. These force fields are ab initio force fields, most parameters were derived based on ab initio data using a least-squares- fit technique developed by Hagler and co-workers [61]. Classical simulations of models using these force fields are possible with either the Discover or Forcite modules. Discover can be used with the COMPASS, PCFF and CVFF force fields. Forcite can be used with the COMPASS, Dreiding and Universal force fields [50].

The goal of a force field is to describe entire classes of molecules with reasonable accuracy. In a sense, the force field interpolates and extrapolates from the empirical data of the small set of models used to parameterize the force field to a larger set of related models. Some force fields aim for high accuracy for a limited set of element types, thus enabling good prediction of many molecular properties. Other force fields aim for the broadest possible coverage of the periodic table, with necessarily lower accuracy. As told before, an important step for molecular simulation is choice of the force field. There are a lot of different force fields available. The choice of the molecular model and the force field for the correct prediction of properties of the system are very important.

Therefore it is inevitable to know about the basic exception, simplification and approximations, which are done in the models. If one is using a molecule system with Coulomb-forces, one has to be aware about the kind of treatment of long-range character of this force. In common it must be said, that there is no "optimal" force field. It depends on the kind of molecular system and the properties of interest. This means that the "modeler" of a molecular system have to know about the weakness and the strengths of the large number of available force fields, to make the right choice.

2.6.2 Differences in force fields used in the study

2.6.2.1 Polymer Consistent Force Field (PCFF)

PCFF (Polymer Consistent Force Field) is intended for application to polymers and organic materials. It is useful for polycarbonates, melamine resins, polysaccharides, other polymers, organic and inorganic materials, about 20 inorganic metals, as well as for carbohydrates, lipids, and nucleic acids and also cohesive energies, mechanical properties, compressibilities, heat capacities, elastic

constants. It handles electron delocalization in aromatic rings by means of a charge library rather than bond increments. In PCFF force field, most parameters were derived based on ab initio data using a least-square-fit technique developed by Hagler and co-workers [62]. Many of the nonbonded parameters of PCFF, which include atomic partial charges and Lennard- Jones 9-6 parameters, were taken from the Consistent Force Field (CFF91). The nonbonded parameters were derived by fitting to molecular crystal data ,based on energy minimization calculations [62-64]. The parameters were developed based on static simulations corresponding to a classical state at 0K, but the experimental data used to determine these parameters were measured at finite temperature. The resulting parameters effectively contain factors such as thermal expansion and vibrational displacements at experimental conditions. Consequently, good agreement between subsequent calculations can be expected when (1) the calculations are performed using an energy minimization method and (2) the experimental data are measured under the conditions that closely approximate those used in the parameterization

2.6.2.2 Compass force field

Compass Force field-based molecular simulation methods can in principle be used to advance chemical and materials research in a number of ways, ranging from their use to gain a qualitative understanding of differences in the behavior of two or more systems, which might result, for example, from small differences in chemical structure, to the opposite extreme in which they are used as a substitute for specific experiments to make quantitative predictions of a range of properties of industrial interest [65].

Hybrid approach consisting of both ab initio and empirical methods was employed to derive a general force field based on the PCFF force field. Most significantly, non-bonded parameters were completely re-parameterized. The outcome was a

new, condensed-phase optimized ab initio force field, called Compass. Compass used in molecular mechanic studies employes the non-bonded terms which includes the soft (9-6) Lennard- Jones potential for the van der waals interaction and a Coulombic term for the electrostatic interactions, are used for interactions between pairs of atoms separated by three or more intervening atoms, or those that belong to different molecules. In comparison with the common LJ- 12-6 function, which is known to be too "hard" in the repulsion region, the LJ-9-6 function is 'softer' but may be too attractive in the long separation range.

In view of the above explanation, we note that both Compass and PCFF force fields use the LJ-96 potential function and also that these force fields use explicit atoms, that is, the vibrations of hydrogen atoms are considered. For Compass force field, the parameters characterizing the remaining non-bonded interactions r and ε are determined using the classical approach. The energy expression may be written as follows:

$$E_{total} = \sum_{b}[k_2(b-b_0)^2 + k_3(b-b_0)^3 + k_4(b-b_0)^4] + \sum_{\theta}[k_2(\theta-\theta_0)^2 + k_3(\theta-\theta_0)^3 + k_4(\theta-\theta_0)^4]$$
$$\sum_{\phi}[k_1(1-\cos\phi) + k_2(1-\cos 2\phi) + k_3(1-\cos 3\phi) + \sum_{\chi}[k_2(\chi-\chi_0)2 + \sum_{b,b'} k(b-b_0)(b'-b'_0) +$$
$$\sum_{b,\theta} k(b-b_0)(\theta-\theta_0)\sum_{b,\phi}(b-b_0)[k_1\cos\phi + k_2\cos 2\phi + k_3\cos 3\phi] +$$
$$\sum_{\theta,\phi}(\theta-\theta_0)[k1\cos\phi + k_2\cos 2\phi + k_3\cos 3\phi] + \sum_{b,\theta} k(b-b_0)(\theta-\theta_0) + \sum_{\theta\theta'\phi} k(\theta-\theta_0(\theta'-\theta'_0)(\phi-\phi_0) +$$
$$\sum_{i,j}\frac{q_i q_j}{r_{ij}} + \sum_{i,j}\varepsilon_{ij}[2(\frac{\sigma_{ij}}{r_{ij}})^9 - 3(\frac{\sigma_{ij}}{r_{ij}})^6] \qquad (20)$$

The first four terms in this equation are sums that reflect the energy needed to stretch bonds, bend angles away from their reference values, rotate torsion angles by twisting atoms about the bond axis that determines the torsion angle, and distort planar atoms out of the plane formed by the atoms they are bonded to. The next

five terms are cross terms that account for interactions between the four types of internal coordinates. The final term represents the non-bond interactions as a sum of repulsive and attractive Lennard-Jones terms as well as Coulombic terms, all of which are a function of the distance r_{ij} between atom pairs. Force fields enable the potential energy of a molecular system to be calculated rapidly and fairly accurately. A typical Force field represents each atom in the system as a single point and energies as a sum of two-, three-, and four-particle interactions.

2.6.2.3 The anatomy of a molecular mechanics force field

The mechanical molecular model considers atoms as spheres and bonds as springs. The mathematics of spring deformation can be used to describe the ability of bonds to stretch, bend, and twist. Non-bonded atoms (greater than two bonds apart) interact through van der Waals attraction, steric repulsion, and electrostatic attraction/repulsion. These properties are easiest to describe mathematically when atoms are considered as spheres of characteristic radii.

The object of molecular mechanics is to predict the energy associated with a given conformation of a molecule. However, molecular mechanics energies have no meaning as absolute quantities. Only differences in energy between two or more conformations have meaning.

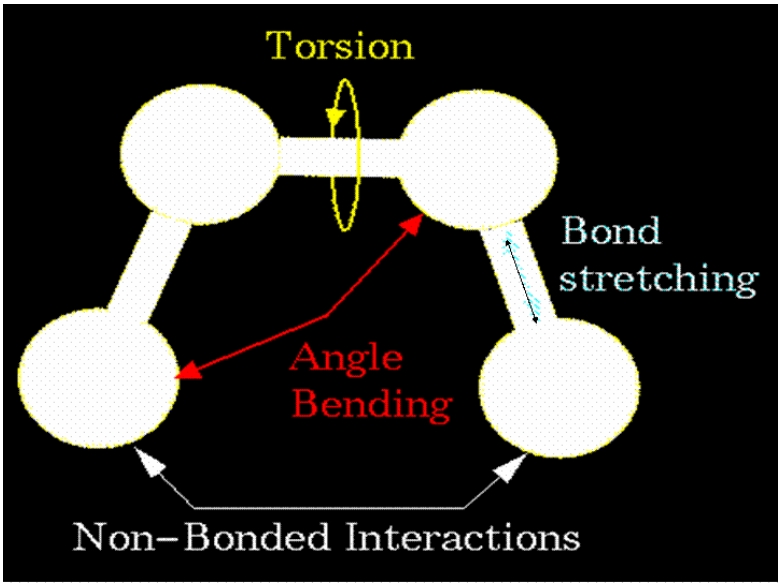

Figure 6. Schematic description of the total Energy of a system [80]

A simple molecular mechanics energy equation is given by:

Total Energy = Stretching Energy + Bending Energy + Torsion Energy + Non-Bonded Interaction Energy (21)

Stretching Energy

$$E = \sum_{Bonds} k_b (r - r_0)^2 \qquad (21.1)$$

Bending Energy

$$E = \sum_{Angles} k_\theta (r - r_0)^2 \qquad (21.2)$$

Torsion energy

$$E = \sum_{Torsions} A[1 + \cos(n\tau - r\phi)] \qquad (21.3)$$

Non-Bonded Interaction Energy

$$E = \sum_i \sum_{j \neq i} \frac{-A_{ij}}{r_{ij}^{6}} + \frac{B_{ij}}{r_{ij}^{12}} + \sum_i \sum_{j \neq i} \frac{q_i q_j}{r_{ij}} \qquad (21.4)$$

with the first and second terms representing the Van der Waals term while the third term represents the Electrostatic term.

The MD technique is used to solve the equations of motion for a system of N-molecules interacting via a potential V, where V is given by: -

$$V(r) = \sum_i V(r_i) + \sum_i \sum_{j>i} V(r_i, r_j) + \sum_i \sum_j \sum_{k>j>i} V(r_i, r_j, r_k + \ldots$$
$$+ \sum_i \sum_j \sum_k)\ldots \sum_N V(r_i, r_j, r_k, \ldots, r_N) \qquad (22)$$

which depends on coordinates of the individual atoms, pairs or triplets. Energy contributions can also be modelled using the relation above.

These equations together with the data (parameters) required to describe the behavior of different kinds of atoms and bonds, is called a force-field. Many different kinds of force-fields have been developed over the years. Some include

additional energy terms that describe other kinds of deformations. Some force-fields account for coupling between bending and stretching in adjacent bonds in order to improve the accuracy of the mechanical model. The mathematical form of the energy terms varies from force-field to force-field.

2.6.3 Lennard-Jones potentials

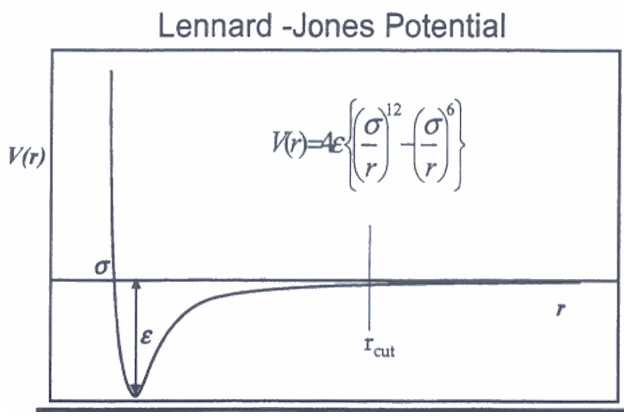

Figure 7. Lennard-Jones Potential

Many of the non bonded parameters of PCFF, which include atomic partial charges and Lennard-Jones 9-6 (LJ-9-6) parameters, were taken from the Consistent force field (CFF91). The non-bond parameters were derived by fitting to molecular crystal data based on energy minimization calculations [62-64]. The parameters were developed based on static simulations corresponding to a classical state at 0K, but the experimental data used to determine these parameters were measured at finite temperature.

The resulting parameters effectively contain factors such as thermal expansion and vibrational displacements at the experimental conditions. Consequently, good agreement between subsequent calculations can be expected when (1) the calculations are performed using an energy minimization method and (2) the experimental data are measured under the conditions that closely approximate those used in the parameterization. The motion of the individual atoms depends on the forces that they exert on each other. This depends on the potential energy, which depends on the distance between two atoms. One of the simplest forms to describe the total energy of atoms is the decomposition into pair potentials, for example in the form of Lennard Jones potentials [65-66]

L-J potentials become useful in describing the interaction between the particles and the polymer and among polymer particles themselves. Combination of attractive and repulsive parts. L-J takes the form:

$$V(r) = 4\varepsilon [(\sigma/r)^9 - (\sigma/r)^6] \qquad (23)$$

Attractive part $\alpha\ 1/r_6$ models induced dipole-dipole interaction (van der Waals interaction). Repulsive part directly proportional to $1/r^{12} = (1/r^6)^2$ was chosen for computational convenience. Where ε and σ are constants; ε is in Joules and σ is in metres. U is the potential energy in Joules and r is the center-to-center distance between two atoms. Details of tiese physical constants are shown in figure 2.2

2.6.4 The need for potentials

Choice of potentials is an inherent part of any model undergoing simulation. The closer the findings match with experimental results, the better the potential. Potentials are virtually always assumed to be pair potentials. Most potential only depend on static quantities (relative position and orientation). Some of the

potentials are many-parameter effective expressions. Their physical significance is limited, but the results can be amazingly good.

2.7 Discover code

It is worth mentioning that throughout the entire study, Accelrys' Discover simulation program has been the core engine of our calculations. It has been very extensively used in all the calculations and has proved to be handling our systems reasonably well. Discover is a user interface to the widely used and well-validated Discover program developed by Accelrys [66]. It is a molecular simulation program for applications in computer assisted molecular design. Discover provides one with the ability to study many more molecular systems and materials types than one could using conventional simulations methods. The insight gained can help one develop and refine working hypotheses, as well as guide your experimental directions.

2.7.1 Discover methodologies for molecular design

Discover is designed for rigorous simulations and incorporates a broad spectrum of molecular mechanics and dynamics methodologies that have demonstrated applicability to molecular design problems [66]. Using one of a range of empirically derived force fields, minimum energy conformations, as well as families of structures and dynamics trajectories of molecular systems, can be computed with confidence.

One can simulate molecules and macromolecules. Periodic boundary conditions allow the simulation of infinite crystals or of solvated systems. Comprehensive analysis features enable the extraction of pertinent results from the simulation. These strategies allow one to address serious projects in computer aided molecular

design. In this study, Energy minimization and Molecular dynamics methodologies were used.

2.8 Data analysis using Molecular Dynamics

When carrying out an MD simulation, coordinates and velocities of the system are saved; these are then used for the analysis. Time dependent properties can be displayed graphically, where one of the axes corresponds to time and the other to the quantity of interest, such as energy, root mean square displacement (rmsd), etc. Other approaches have been developed for representing the dependence of angle rotation (dihedrals). Average structures can be calculated and compared to experimental structures.

2.9 Radial distribution functions

The Radial Distribution Functions (rdf's) are a very useful way of describing the structure of a system [67] and the information can be extracted from MD simulations via the pair distribution function, g(r), which is given by

$$g_{ij}(r) = \{\frac{\langle n_{i_j}(r)\rangle}{4\pi r^2 (n_i n_j)^{\frac{1}{2}}}\} \qquad (24)$$

where $<n_{ij}(r)>$ is the ensemble average of the number of species of type j in a radial shell of r with a species of type i at the centre, n is the bulk density of ion type i [68]. The pair distribution function, g (r), is the probability of finding an atom or molecule at a distance r from another atom or molecule compared to the ideal gas distribution. Thus g(r) is dimensionless. Higher radial distribution functions like the triplet radial distribution functions can also be found, but they

are rarely calculated and so in most cases the references to the rdf's are usually taken to mean the pair wise version. In a crystal rdf's has an infinite number of sharp peaks whose separations and heights are characteristics of the lattice structure. rdf's can be measured experimentally using the X-ray diffraction where a regular arrangement of the atoms in a crystal gives the characteristics x-ray diffraction pattern with bright and sharp spots [69].

2.9.1 Calculation of radial distribution functions (rdf's)

The local structure of the system can be described by the pair correlation or radial distribution function g(r). Of course, molecules are in constant motion, rotating and moving about in erratic ways, so the notion of structure has meaning
only in an average sense. There are many possible ways to quantify this average structure. The radial distribution function (or rdf) is one such way and is one of the most important. The rdf is important for three reasons:
-For pair wise additive potentials, knowledge of the rdf is sufficient information to calculate thermodynamic properties, particularly the energy and pressure
-The rdf can be measured experimentally, using neutron-scattering techniques.
The rdf addresses the question, "given that I have one atom at some position, how many atoms can I expect to find at a distance r away from it? - more precisely, we ask for the number of atoms at a distance between r to r + dr. This idea can be represented as shown in figure 2.3.

The darkened atom at the centre is the reference atom, and the circle around it represents the other atoms. A ring centred on the reference is drawn with radius r and thickness dr, and in this example, three atoms are positioned in this ring and highlighted.

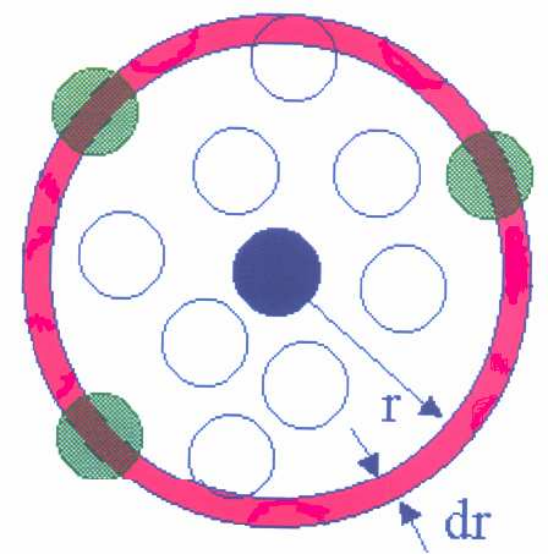

Figure 8. Diagrammatic representation of rdf

In Figure 9, we show the Radial Distribution Function of liquid argon from a molecular dynamics simulation. A few number of peaks can be observed and g(r) is observed to be zero at small values of r [70].

The radial distribution function can be an effective way of describing the structure of a system at different temperatures. Differentiation between a solid, liquid and a gas can be made using the rdfs by the number of peaks appearing in a particular rdf plot. In a crystal, the radial distribution functions have a multiple number of sharp peaks whose separations and heights are characteristic of the lattice structure. The radial distribution function of a liquid is an intermediate between the crystal and the gas, with a small number of peaks at short

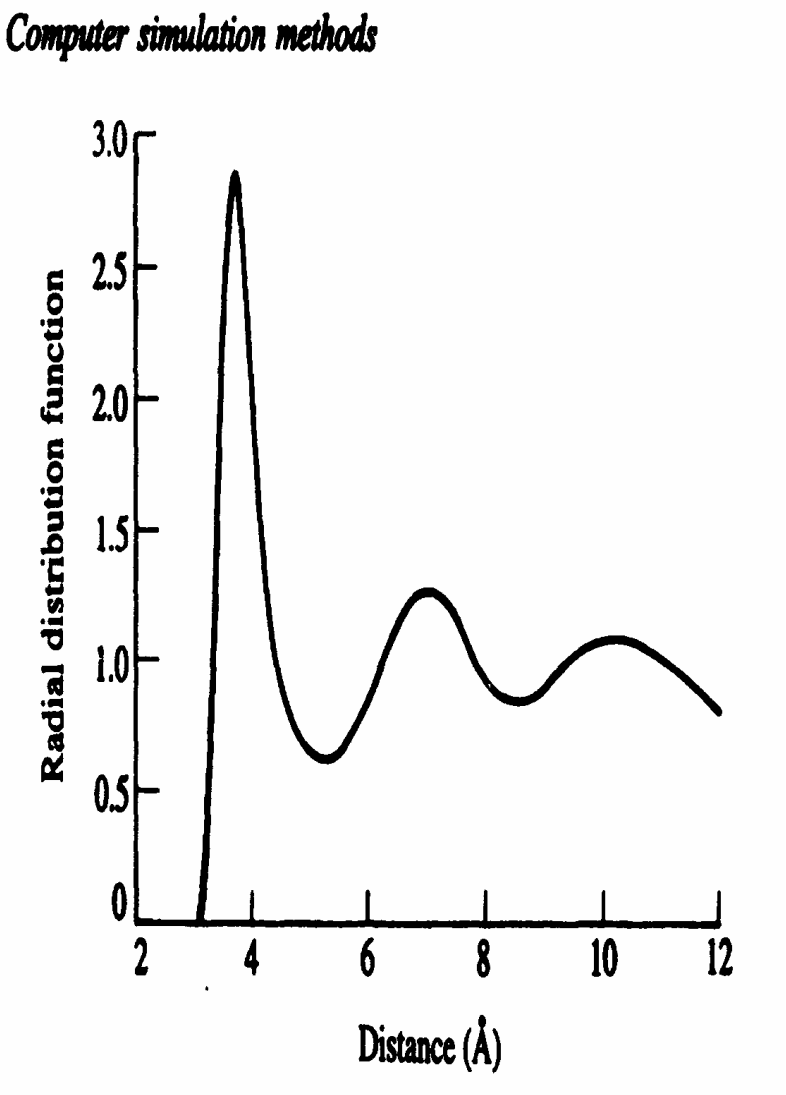

Figure 9. The radial distribution function of a liquid argon from a molecular dynamics simulation

distances, superimposed on a steady decay to a constant value at longer distances. The rdfs for a gas usually have a single clearly defined peak and then short range peaks as the distance is increased [71].

2.9.2 Mechanical Properties

We have used molecular dynamics simulation to investigate the mechanical properties of cellulose before and after introducing water. Discover mechanical properties calculations were performed using the static formula approaches. Some analysis was carried out on the MD run structures and the corresponding properties were determined.

In classical mechanics, the Young's modulus is defined as:

$$Y = \frac{1}{V_0}\frac{\partial^2 E}{\partial \varepsilon^2}, \qquad (25)$$

Where V_0 is the equilibrium volume, E is the strain energy, and ε is axial strain.

From solid mechanics, the Poisson's ratio of a material can be calculated from the relation:

$$\nu = (Y/2 - G)/G \qquad (26)$$

where Y is the Young's modulus and G, the shear moduli [72].. Using the data from our simulated results, and by employing equation (26), we calculated the Young's modulus of all celluloses. Using Discover code discussed earlier in this chapter, the Young's modulus and Poisson's ratio can be computed using least-squares fit to the averaged tensile stress vs. tensile strain, and to the average lateral

strain vs. tensile strain. The .out file contains summary of the elastic properties i.e. bulk, and shear moduli are derived according to equations 27 and 28.

and Bulk modulus, $K = \lambda + 2/3\ \mu$ (27)

The shear modulus is given by $G = \mu$ (28)

Chapter 3

3 Structural and Mechanical properties

3.1 Introduction

In this chapter we present and discuss results on structural and mechanical properties of cellulose allomorphs obtained using the methods described in the previous chapter. In cases where experimental data is available comparisons will be made. Most results were generated by Discover code coupled with the Compass Force Field and Polymer Consistent Force Field (PCFF). We confined our study to four allomorphs of cellulose, namely cellulose Iβ, cellulose II, cellulose III, cellulose IV_1 and IV_2. In the following sections, we report results on structural properties of various cellulose allomorphs. Lattice parameters were calculated for pure systems, and systems with different water concentrations. Effect of pressure on the lattice parameters will also be reported. Dihedral angles, radial distribution functions (rdf's) for pure systems and at different water concentrations will also be discussed. And lastly, we shall report and discuss calculated mechanical properties of various celluloses at different water concentrations.

3.2 Structural properties

3.2.1 Lattice parameters

Lattice parameters for five cellulose polymorphs were calculated at 300K using atomistic simulation techniques. MD calculations were carried out with the Discover program of Accelrys molecular modelling package [66] The Compass force field was

Structures	Cell length			Cell angles		
	a(Å	b(Å)	c(Å)	α(°)	β(°)	γ(°)
Iβ	7.81	8.45	10.47	90.00	90.00	94.75
II	8.31	9.25	10.94	90.00	90.00	116.79
III	10.25	7.78	10.34	90.00	90.00	122.40
IV_1	7.79	8.39	10.92	91.65	89.61	88.18
IV_2	8.03	8.38	11.21	89.98	89.92	89.61

Table 2. Compass force field energy minimized lattice parameters for celluloses

used to perform the geometric optimizations and molecular dynamic simulations on all species. The conjugate gradient algorithm has been used for the minimization of all the systems. Brief energy minimization of 5000 steps was performed, followed by the molecular dynamics simulation of 10000 time steps (10ps) at NPT conditions to equilibrate the structure. Starting from around 2 ps, the temperature and total energy remain constant over long periods, which indicated that the systems were fully equilibrated. Then a further NPT ensemble production molecular dynamics simulation trajectory of 10 ps was created from which all the properties discussed in this work were calculated. Berendsen thermostat was used to control the temperature. The parameters mentioned above were applicable in calculations for all the structures. We noted, however, that even after equilibration, there was no change in the results we obtained after minimization; hence the result presented in this chapter represents the both calculations. Calculations were carried out at temperatures 300K. Moreover, calculations for rdf's and mechanical properties (without water) were performed at temperatures 300K, 500K and 700K.

Energy Minimization and Molecular Dynamics results are shown in tables 2 and 3, respectively. In table 3 we further show a comparison between experimental and calculated lattice parameters for systems without water using Compass force field and the results are broadly discussed below. Table 4 shows percentage difference of lattice parameters from MD simulations and experiments for various cellulose types.

The calculated lattice parameters are for systems without water and were carried out at 300K. As for cellulose Iβ, the **a** and **b** parameter were -0.3% and 2.0%, higher than experimental, respectively, while the **c** parameter was 0.6% higher. Cellulose II had parameters, **a, b** and **c** 3.3%, 2.6 and 7.4% higher than experimental. Cellulose III had the **a** and **b** parameters -8.5%, -1.4% lower than experimental with the c parameter 1.8% higher, and the alpha-angle was 12.6% higher than experimental. The cell parameters for cellulose IV_1 and IV_2 were well reproduced except for the **c** parameters of cellulose IV_2 as can be seen in the percentage differences (table 4). Further, it was noted that meanwhile cell lengths were changing; we observed some changes also in the cell angles for various celluloses. This was noted for both minimization and MD results, thus leading to the changes that were noted in the cell volumes. Generally, our calculated results, both lattice parameters and cell volumes, are in reasonable agreement with the experimental values. Also shown in table 4 are the percentage differences in volumes, last column. These percentage differences are between systems without water and experimental volumes (in table 3). Cellulose Iβ, II and III were -0.3%, 9.0 and 7.0 % respectively, lower than experimental data, while those for Cellulose IV_1 and IV_2 were found to be 10.1% and 11.5% higher than experimental results. We further conducted some calculations of lattice parameters and volumes using PCFF (see table 5) and we managed to reproduce the results that were reasonably comparable with experimental results.

Kroon-Batenburg et al [70] reported on molecular dynamics (MD) calculations of cell dimensions for cellulose I as **a**= 8.17 Å, **b**= 7.86 Å, **c**= 10.38 Å and **γ**= 97.0° and cellulose II as having **a**= 8.01 Å, **b**= 9.04 Å, **c**= 10.36 Å and **γ**= 117.1°. These results also accord very well with our predictions. Several authors have suggested that unit cell of the native cellulose may depend on the source.

	Experimental [Ref 22]			Compass		
	Cell lengths (Å)	Cell angles (°)	Volume ($Å^3$)	Cell lengths (Å)	Cell angles (°)	Volume ($Å^3$)
Iβ	a =7.85 b= 8.27 c=10.38	α = 90.00 β= 90.00 γ= 96.30	692.3	a=7.82 b=8.44 c=10.45	α= 89.65 β = 89.88 γ = 94.53	689.7
II	a =8.10 b= 9.03 c=10.31	α =90.00 β =90.00 γ= 117.10	788.5	a=8.37 b=9.27 c=11.08	α= 90.22 β= 90.04 γ=116.68	859.6
III	a=10.25 b=7.78 c=10.34	α=90.00 β=90.00 γ=122.40	706.9	a= 9.37 b= 7.67 c= 10.53	α = 101.38 β= 80.36 γ =115.03	756.7
IV_1	a =8.03 b =8.13 c=10.34	α = 90.00 β = 90.00 γ =90.00	672.4	a=7.99 b= 8.36 c= 11.09	α= 90.72 β = 90.79 γ =90.56	740.7
IV_2	a= 7.99 b =8.10 c=10.34	α =90.00 β =90.00 γ =90.00	673.1	a=8.03 b=8.34 c=11.21	α = 89.43 β = 89.01 γ =90.67	750.7

Table 3. Comparison between experimental and molecular dynamics calculated lattice parameters

Unit cell	a %	b %	c %	α %	β %	Γ %	Volume (Å^3)
Iβ	-0.3	2.0	0.6	0.3	-0.1	-1.8	-0.3%
II	3.3	2.6	7.4	0.2	0.0	0.3	9.0%
III	-8.5	-1.4	1.8	12.6	-10.7	-6.0	7.0%
IV_1	0.4	2.8	7.2	0.8	0.8	0.6	10.1%
IV_2	0.5	2.9	8.4	-0.6	-1.1	0.7	11.5%

Table 4. The percentage difference in the corresponding unit cell parameters and volumes between the experimental and the MD simulated structures using compass force field

Cellulose	Cell lengths (Å)	Cell angles (°)	Volume (Å^3)
Iβ	a=8.05 b=8.36 c=10.71	α = 91.45 β = 82.51 γ = 97.08	720.3
II	a=8.43 b=8.87 c=10.56	α = 90.00 β = 90.00 γ = 117.79	789.6
III	a= 8.88 b= 8.62 c= 10.58	α = 92.40 β = 88.73 γ = 116.21	809.8
IV_1	a=8.07 b=8.31 c=10.72	α = 90.51 β = 89.45 γ = 96.56	718.9
IV_2	a=7.93 b=8.53 c=10.66	α =97.74 β = 79.13 γ = 98.27	721.1

Table 5. MD calculated PCFF lattice parameters and the corresponding volumes

Unit cell	a %	b %	c %	α %	β %	γ %	Volume ($Å^3$) percentages
Iβ	2.5	1.0	3.1	1.4	-8.3	0.8	4.0
II	4.0	-1.7	2.4	0.0	0.0	0.5	0.1
III	-13.3	10.7	2.3	2.6	-1.4	-5.0	14.5
IV_1	0.4	2.2	3.6	0.5	-0.6	6.7	6.9
IV_2	-0.7	5.3	3.0	8.6	-12.0	9.1	7.1

Table 6 Percentage difference in the corresponding lattice parameters and volumes between the experimental and the MD simulated structures using PCFF

Table 6 shows the percentage differences for cell parameters generated by PCFF. Although Compass force field was preferred for generating most of the results in this study, and results are generally good, we observed that percentages for lattice parameters and volumes (table 4 and 6) proved otherwise as there are higher deviations for compass than we noticed for PCFF. However, from these calculations; we noted that Compass force field reproduced cell parameters that are systematic.

Comparing the percentage differences in cell volumes, tables 4 and 6 (i.e. Compass and PCFF), one notices that cellulose III records 14.5% higher compared to 7.0% obtained using Compass force field. However, Compass force field, however records an increase in volume percentage differences from cellulose III to cellulose IV_2. Water cannot penetrate crystalline cellulose; however dry amorphous cellulose absorbs water, hence becoming soft and flexible. Some of this water is non-freezing but most is simply trapped.

3.2.2 Cell parameters for cellulose structures with water

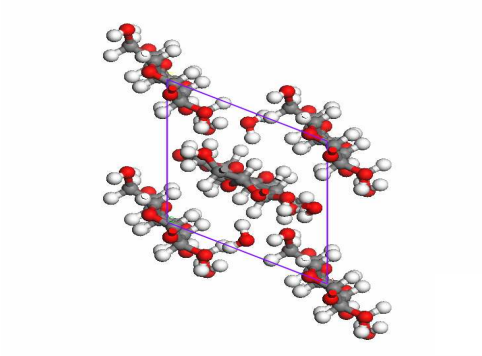

Figure 10. Simulated cellulose Iβ crystal structure with water molecules

Cellulose	One water molecule per unit cell			Two water molecules per unit cell		
	Cell lengths (Å)	Cell angles (°)	Vol. (Å^3)	Cell lengths (Å)	Cell angles (°)	(Å^3)
Iβ	a=8.54 b=8.20 c=10.40	α =89.99 β =89.99 γ =93.35	747.0	a=9.36 b=7.92 c=10.44	α = 89.87 β =90.12 γ =79.12	846.9
II	a=8.60 b=8.82 c=10.40	α = 90.0 β = 89.99 γ =116.34	734.3	a=8.61 b=9.02 c=10.28	α = 97.72 β = 89.24 γ =103.16	827.0
III	a=12.10 b=7.11 c=10.34	α =86.26 β =88.82 γ =111.83	848.9	a=11.76 b=9.79 c=10.39	α =106.98 β = 103.89 γ =114.95	930.2

IV_1	a=9.14 b=8.21 c=10.56	α =97.28 β =95.27 γ= 95.66	722.8	a=11.65 b=8.38 c=10.35	α = 99.22 β =102.68 γ =93.22	773.9
IV_2	a=9.14 b=8.21 c=10.56	α =85.32 β=108.84 γ =75.13	698.9	a=11.65 b=8.38 c=10.35	α =99.63 β =106.97 γ =119.66	730.1

Table 7. Calculated lattice parameters for cellulose (Iβ -IV2) after wetting

Less water is bound by direct hydrogen bonding if the cellulose has high crystallinity but some fibrous cellulose products can hold on to considerable amount of water in pores; water holding ability correlating well with the amorphous and void fraction (*i.e.* the porosity).

Czihak et al [1999], though he studied amorphous polymer, highlighted that the water interactions are dominated by hydrogen bonding with OH group, hence water is adsorbed by the disordered (amorphous) regions of cellulose as they contain non-saturated OH groups. However, cellulose under investigation is in crystalline form, thus OH groups are less exposed to solvent (water) as it is the case with amorphous cellulose. Table 7 shows the variation of calculated lattice parameters and volumes of various cellulose structures with increasing water molecules. One and two molecules of water per unit cell as shown in figure 10 were introduced consecutively, and MD calculations were performed.

The **a** parameter (cellulose Iβ), and **b** parameter (cellulose II) show an increase with increasing number of water molecules, though not consistently. Other parameters showed an inconsistent response with an increase in the number of water molecules.

Currently there are no experimental results to compare our calculated properties with. When the second molecule was introduced, the parameters showed a decrease. Cellulose II shows an increase with one molecule except the **c** parameter which did not show much variation. When two molecules

Cellulose type	Deviation from experiment	Deviation from MD (one molecule)	Deviation from MD (two molecules)
Iβ	-0.3%	8.3%	22.8%
II	9.0%	-14.5%	3.8%
III	7.0%	12.1%	-3.5%
IV_1	10.1%	-2.4%	4.4%
IV_2	11.5%	-6.9%	-2.7%

Table 8. Percentage differences of cell volumes for various cellulose types without water and at different water concentrations

of water were introduced, we note that the **b** parameter and angle alpha have increased significantly, which is due to cellulose swelling, while the gamma angle had reduced substantially. Percentage differences for volumes of various cellulose types at different water concentrations are shown in table 8. The third and fourth columns show the percentage differences between the volumes of various cellulose types with one and two molecules of water, respectively.

It was observed that the percentage difference for celluloses Iβ, II,IV_1 and IV_2 increases with addition of water molecules, except for cellulose III which shows a decrease from 12.% to -3.5% with increasing water concentration. These percentages, when compared with calculations without water, one notice that

celluloses Iβ and III were increasing when one molecule of water was added, while for celluloses II (9.0% to -14.5%) and IV_1 (11.5% to -6.9%) we see a decrease in percentages when water was added.

3.2.3 The effect of pressure on the volume and lattice parameters

Pressure (GPa.)	Volume ($Å^3$)				
	Iβ	II	III	IV_1	IV_2
10 GPa	521.19	609.42	695.90	527.230	570.19
20 GPa.	478.16	571.36	636.70	480.42	527.30
30 GPa.	447.56	530.44	649.40	454.21	494.91

Table 9 .Pressure variation with respect to volume

Calculations on pressure variation with respect to volume were carried out as shown in table 9. We observe that as the pressure increases, a decrease in the volume occurs, except for cellulose III at 30 GPa. This trend was noted for various cellulose types studied.

In order to study the behaviour of the various cellulose types when subjected to pressure, we calculated lattice parameters of all five systems at various pressures and the results are shown in table 10. From the table, we observed that the lattice parameters contract when subjected to pressure, and it is common knowledge that these imply change in the volume of the systems with respect to pressure. However, there is currently no experimental data available, to our knowledge.

	Lattice parameters (Å, °)				
	Iβ	II	III	IV_1	IV_2
10 GPa.	a=6.679 b=7.625 c=10.234 α =90= β, γ=97.205	a=7.550 b=8.114 c=9.948 α =83.191 β =79.384 γ =117.904	a=8.309 b=8.179 c=10.240 α =94.352 β =85.747 γ =116.777	a=7.138 b=7.324 c=10.085 α =97.866 β =90.920 γ =93.704	a=7.631 b=7.382 c=10.122 α =101.793 β =86.204 γ =109.722
20 GPa.	a=6.376 b=7.504 c=9.994 α =90= β γ =101.137	a=7.410 b=7.902 c=9.758 α =96.936 β =101.787 γ =118.811	a=8.053 b=7.832 c=10.095 α =95.250 β =83.283 γ =118.552	a=6.803 b=7.171 c=9.848 α =97.800 β =86.761 γ =93.343	a=7.213 b=7.236 c=10.103 α =102.600 β =86.444 γ =111.228
30 GPa.	a=6.040 b=7.416 c=9.992 α =90= β γ =101.034	a=6.995 b=7.838 c=9.675 α =81.108 β= 80.026 γ =117.514	a=8.117 b=7.956 c=10.056 α =78.010 β =91.209 γ =123.295	a=6.703 b=6.943 c=9.760 α =100.571 β =83.566 γ =93.477	a=7.007 b=7.113 c=9.930 α =101.810 β =85.357 γ =112.251

Table 10. Variation of lattice parameters with respect to pressure

Figures 11-15 show the plots of lattice parameters against pressure for various cellulose types. As can be seen from, table 10, cellulose Iβ, complemented by

figure 11, lattice parameters shows a decrease in the parameters **a**, **b** and **c** with an increase in pressure. However, the decrease was not linear, hence different slopes are observed.

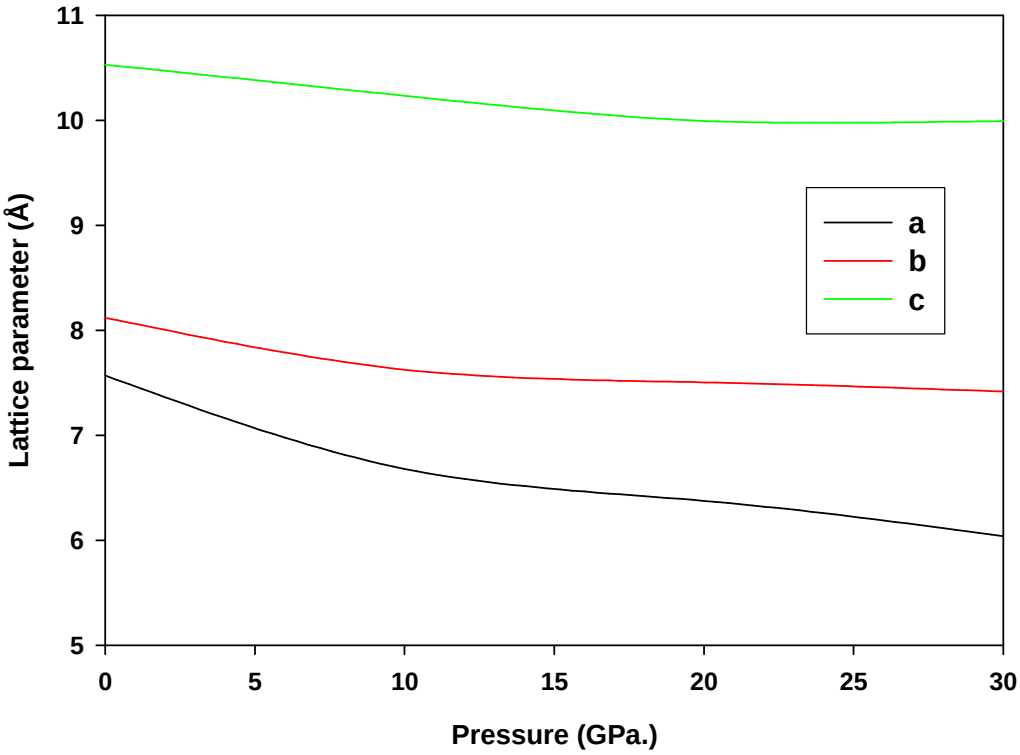

Figure 11. Lattice parameters against pressure for cellulose Iβ

As for cellulose II, figure 12, the same trend as in cellulose Iβ was observed, but with the **a** parameter decreasing significantly at 20GPa. However, cellulose III, figure 13, contrary to the behaviour depicted in cellulose Iβ and II, the **a**, parameter appears to have been more compressed than the **b** parameter. A gentle increase in the **a** and **b** parameters was observed at 20GPa, although all the parameters were generally decreasing with an increase in pressure. Cellulose IV_1, figure 14 shows similar trend observed in figures 11 and 12, while cellulose IV_2 depicts the behaviour different from other cellulose types. In this case, the **a** exceeded the **b** parameter in the pressure range 4-19GPa. The **c** parameter was

noticeably greater than the **a** and **b** parameter in all cellulose allomorphs. One interesting trend noted in all lattice parameters of most celluloses with pressure is a change in slope at approximately at 10GPa and 20GPa

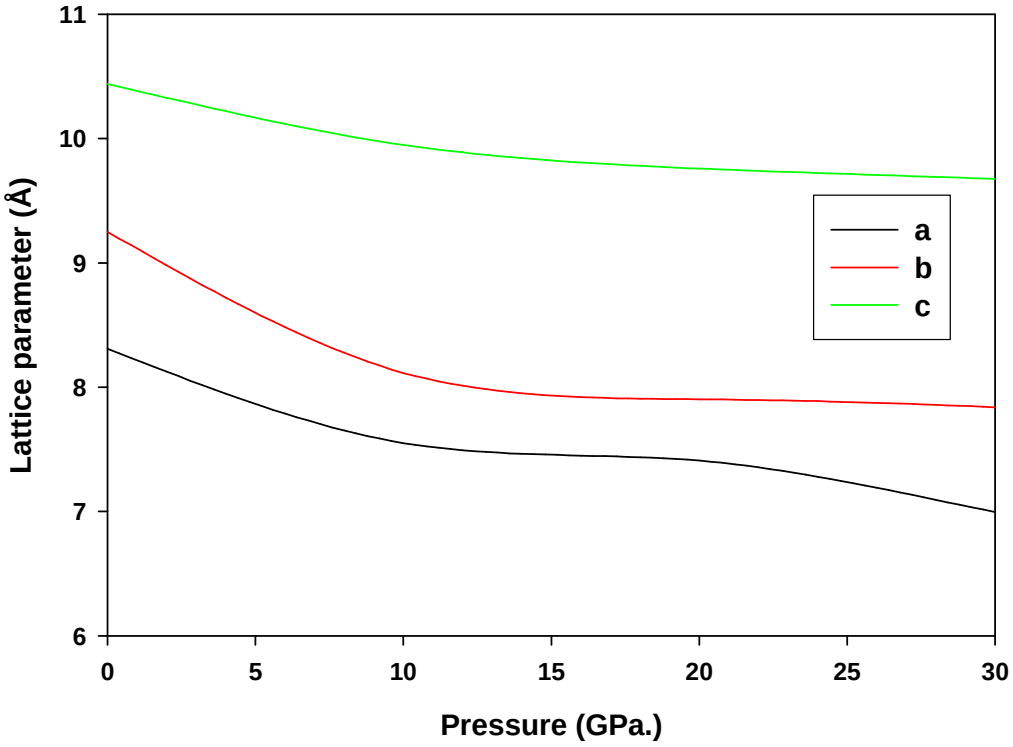

Figure 12 Lattice parameters against pressure for cellulose II

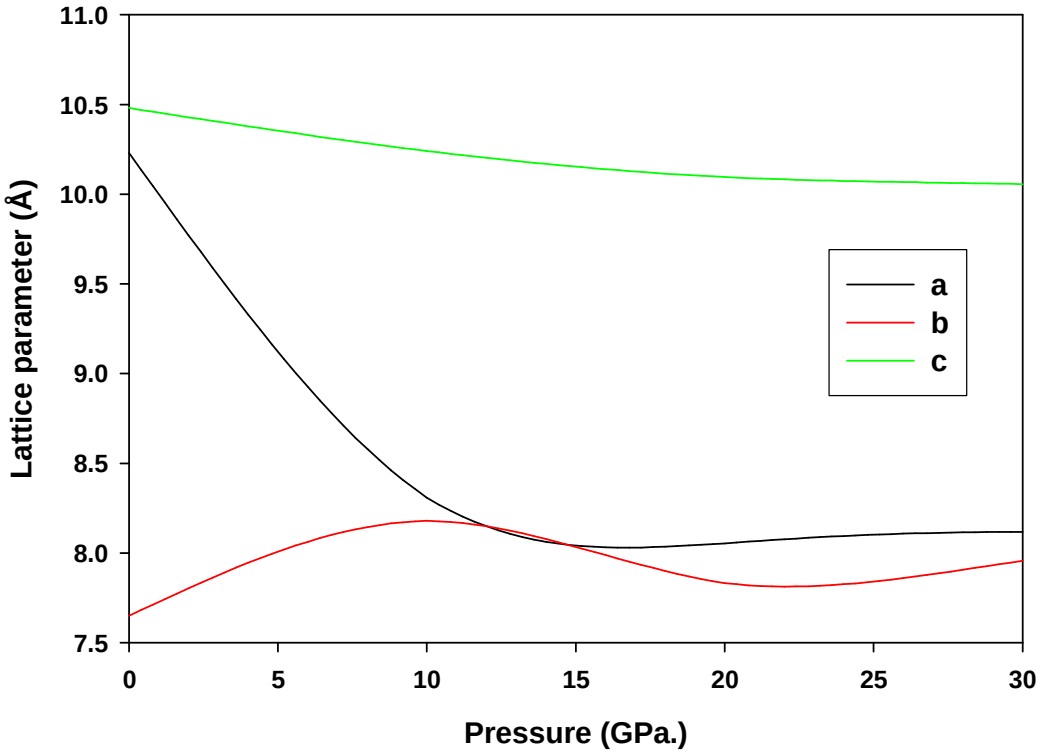

Figure 13. Lattice parameters against pressure for cellulose III

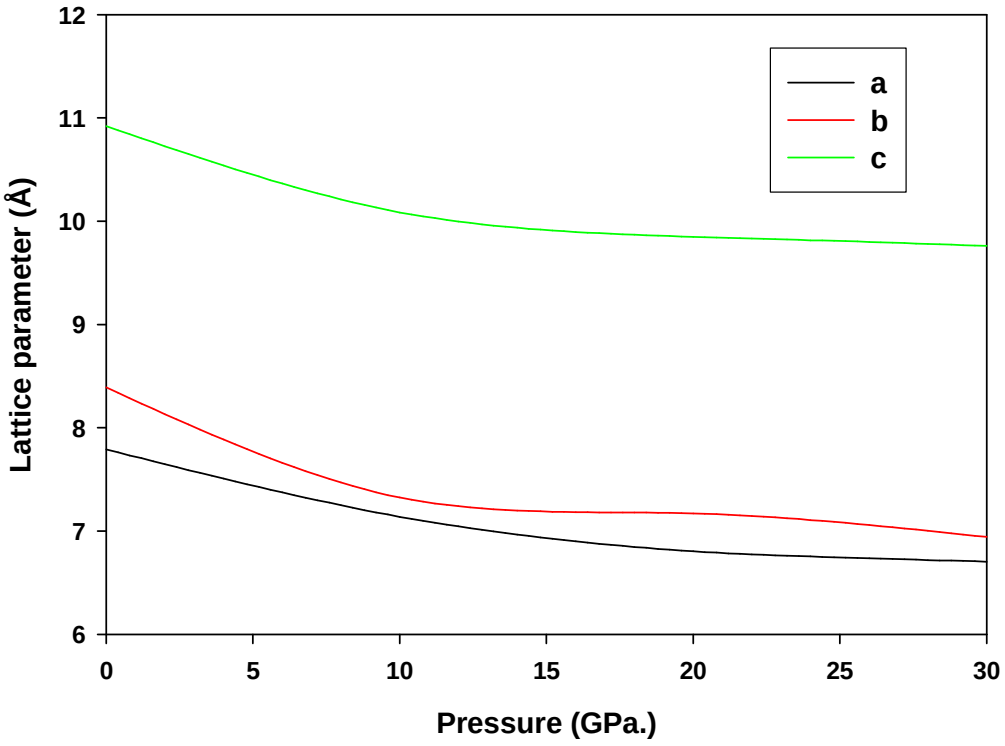

Figure 14. Lattice parameters against pressure for cellulose IV_1

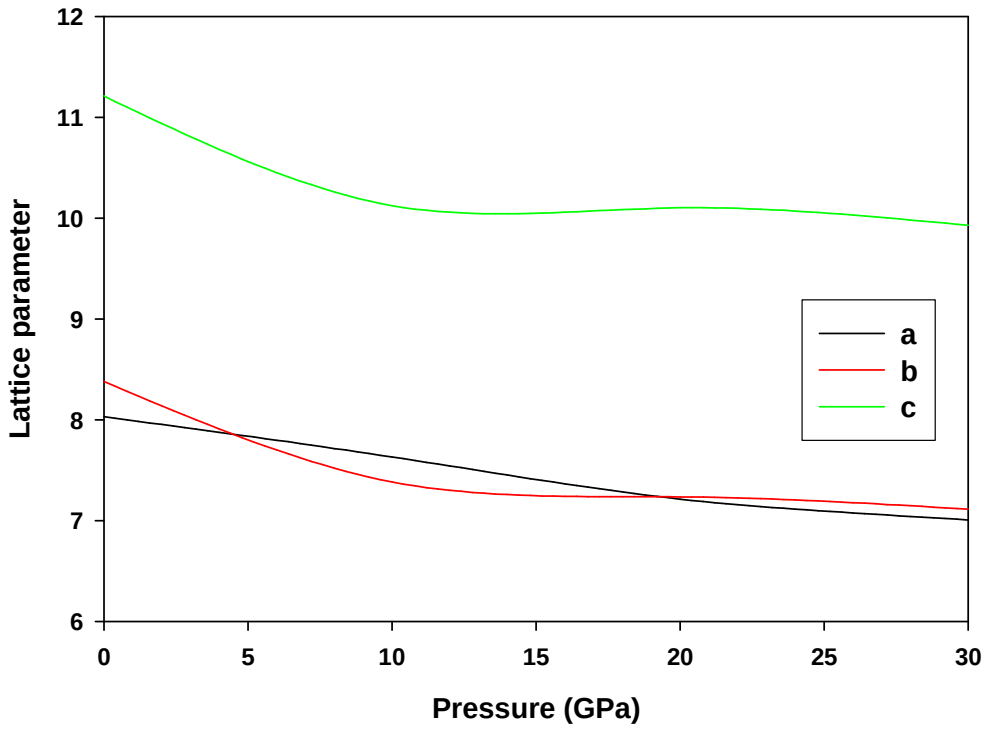

Figure 15. Lattice parameters against pressure for cellulose IV_2

3.3 Dihedral angle distributions

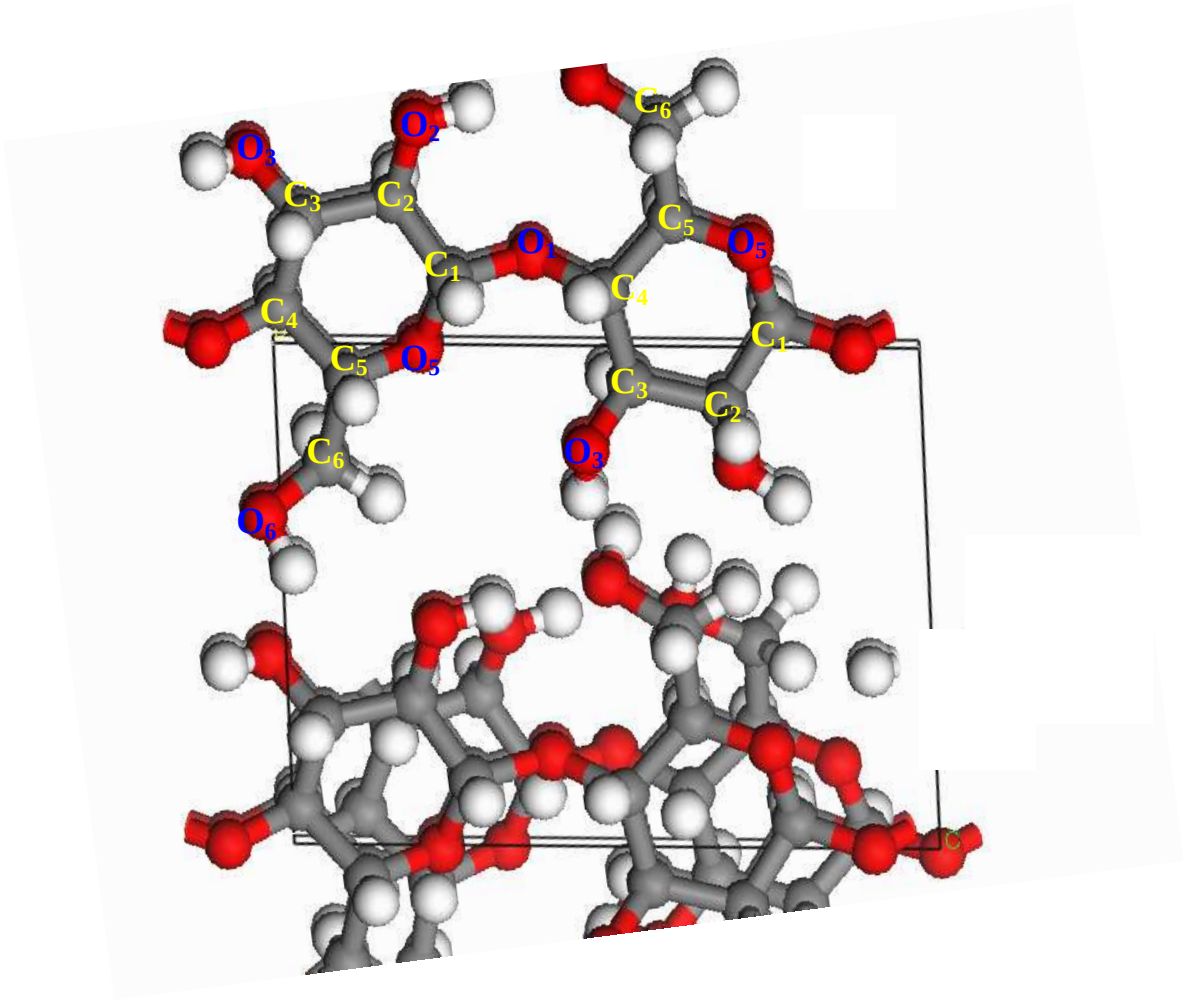

Figure 16. Naming convention for atoms in cellulose

MD simulations were carried out to calculate dihedrals for the quartet (O5-C1-C2-O3) through to C5-O5-C1-C2, as indicated in table 11, for cellulose Iβ through to cellulose IV_2. These labels are shown in figure 16. We note here, the main difference found for cellulose II in which the initial structure had dihedral angle of 72.31º for the O5-C1-C2-O3 quartet. However, Naidoo and Brady [70] computed some ring dihedrals for the chain conformation of the disaccharides, and they

obtained 54.09º, -51.23º, 53.25º, -57.46º, 62.25º and -60.97º for similar quartets. Using these data, we calculated the standard deviation from these values and were found to be 62.1. The averages from dihedrals of the quartets from table 11 are found to be 54.11º, -46.88º, 48.22º, -56.91º, 60.01º and 59.37º for celluloses Iβ, II, III, IV_1 and IV_2, respectively. These averages were obtained by averaging all dihedral angles for all the quartets for each cellulose type. The standard deviation for this set of values was calculated and amounted to 24.87, less than the value we obtained from Naidoo's work. There was a reasonable correlation between the averages from our calculations and those obtained by Naidoo et al in their study on disaccharides.

Dihedral identity	Iβ	II	III	IV_1	IV_2
O5-C1-C2-C3	45.38	63.10	57.76	41.21	63.10
C1-C2-C3-C4	-35.51	-58.12	-52.77	-35.38	-52.62
C2-C3-C4-C5	42.40	50.35	53.24	48.19	46.95
C3-C4-C5-O5	-60.76	-51.92	-55.32	-61.82	-54.77
C4-C5-O5-C1	58.06	53.69	61.48	54.24	72.59
C5-O5-C1-C2	–52.34	-56.65	-65.27	-48.77	-73.84

Table 11. Calculated dihedral angles for the $^4C_1$ chain conformation

3.4 The variation of rdf's with temperature for systems without water

Radial Distribution Functions (RDF's) were introduced in section 2.11, and are valuable in describing the structure of a system and can be extracted from MD simulations via pair distribution functions, g(r). Molecular dynamics technique using Discover code and Compass Force Field were used to calculate the radial

distribution functions for cellulose structures at various temperatures. The plots show the variation of pair distribution functions with distances where the minimum and maximum peaks of the systems can be clearly defined. A well defined peak that is obtained shows the successive nearest neighbour distances. The peaks and radial distances in the following rdf's have been labelled as follows: 0.9 Å -1.2 Å (C-H, O-H), 1.4 Å -1.6 Å (C-C, C-O). This labelling (at 300K) will apply also to rdf"s at higher temperatures (500K and 700K)

The radial distribution functions for cellulose Iβ-IV_2 at different temperatures are given in figures 17-21. Figure 17 shows the radial distribution function or pair correlation function g (r) of cellulose Iβ. In the region 0.9 Å -1.2 Å (C-H, O-H), we see sharp peaks which disappear in the region 1.2 Å -1.4 Å and emerge in the region 1.4 Å -1.6 Å (C-C, C-O). In this region, 1.4 Å -1.6 Å (C-C, C-O), we see that the peaks become broader than it was the case in the region 0.9 Å -1.2 Å(C-H, O-H). The maximum peak occur at r = 1.1 Å (O-H). The sharp peaks indicate a more ordered system. The rdf's shown exhibit peak broadening with increasing temperature and this indicates a greater degree of disorder at higher temperatures. At lower temperatures the heights of the peaks increase and their broadness decreases, which depicts a more ordered system due to less thermal motions of atoms and also phase changes. However, the melting point of cellulose is undefined and a supercell is necessary for one to see this.

Figure 18 shows rdf's of cellulose II at different temperatures. In the region 1.9 Å -1.2 Å (C-H, O-H) we see that there are sharp peaks at around 0.9 Å (C-H) and 1.1 Å (O-H) respectively, indicative of a high ordered systems. The maximum peak is observed at 1.1 Å (O-H). All the peaks disappear in the region 1.2-1.4 Å and emerge in the region 1.4 Å -1.6 Å (C-C, C-O). Interesting to note, is the peak broadening with an increase in the temperature, which is due disordering of the system. Again in this region 1.4 Å -1.6 Å (C-C, C-O), we observe that the peaks in

coalesce with increasing temperature, hence no many more peaks in this region. Cellulose III (Figure 19) shows the maximum peak at r = 1.1 Å (O-H), and other sharp peaks at around r = 1.0 Å (C-H) and 1.1 Å (O-H) at 300K and 500K. A sharp peak indicates a crystalline system where atoms are intact. These peaks diminished in the region 1.2 Å -1.4 Å and emerge in the region 1.4 Å -1.6 Å (C-C, C-O) . The effect of temperature was also observed where we see peaks broadening and coalescing as the temperature increases.

Except for cellulose IV_2, however, sharp peaks were obtained again at around r = 1.4 Å (C-C) in all the systems. Heiner et al [73], who studied cellulose Iα and Iβ, reported that it has probably to do with the differences in the hydrogen bonding. Chen et al [5] reported on rdf's calculated for amorphous cellulose models as well as for crystal models for cellulose I and cellulose II in order to identify any long range order in the amorphous cellulose models. One fundamental difference between crystalline and amorphous states is the existence of long range order found only in the former. In agreement with our work, Chen obtained the rdf for celluloses I and II which had four large peaks around 1.0 Å -1.5Å, which correspond to C-H, O-H, C-C and C-O bond lengths. In addition they obtained many smaller peaks between 2.0 Å and 3.0Å, which included the hydrogen bonding atom distances. In our work, these peaks diminish at around 1.2 Å -1.4Å for the same structures in crystalline form. Hence, we did not observe any definite peaks beyond 1.6 Å. The large peaks observed by Chen et al [73] for cellulose I and II at 3.0 Å are due to the periodic repetition of structural units and can thus be considered as evidence of long range order. Cellulose IV_1 in figure 20 shows the maximum peak at r = 1.1 Å (O-H), which then disappears and emerges in the region 1.4 Å -1.6 Å (C-C, C-O). We further observe peaks broadening and coalescing with an increase in temperature. Cellulose IV_2 (figure 21) shows the maximum peak at r = 1.1 Å (O-H), which diminish at distances 1.2 Å -1.4 Å,

after-which several peaks appear. We noted that the peaks broaden and coalesce on heating, which is indicative of thermal motion of atoms.

The systems in this study show a series of well defined peaks corresponding to successive nearest neighbour distances. The first highest peaks occurs at r = 0.9 Å (C-H) and maximum peaks occur at r = 1.1 Å (O-H) for all the systems. The maximum peaks emerge at a r = 1.4 Å (C-C), except for cellulose IV_2 where the peaks in the region 1.4 Å -1.6 Å (C-C, C-O) are not well defined. The multiple sharp peaks occur in the regions 0.9 Å -1.2 Å (C-H, O-H) in all the systems and these peaks are indicative of the crystalline state of the system. Another common trend is that the systems show disorder in the region 1.4 Å -1.6 Å (C-C, C-O). It was also noted that the peaks diminish in the radial distance r =1.2 Å and emerge at r =1.4 Å (C-C) for all the systems. The long-range order clearly indicates that the structure is still crystalline and is ascribed to a strong interaction caused by the hydrogen atoms. The profile of peak broadening indicates a greater degree of disorder at higher temperatures. Therefore the temperature has an effect on cellulose structures; the higher the temperature, the higher the disorder in the system and the broader the peaks. At distances beyond 1.6 Å, the rdf's in all cellulose types are not clearly distinguishable indicating differing environments in each phase**.** Generally, we see that for all systems, there is a decrease in the peak heights at larger

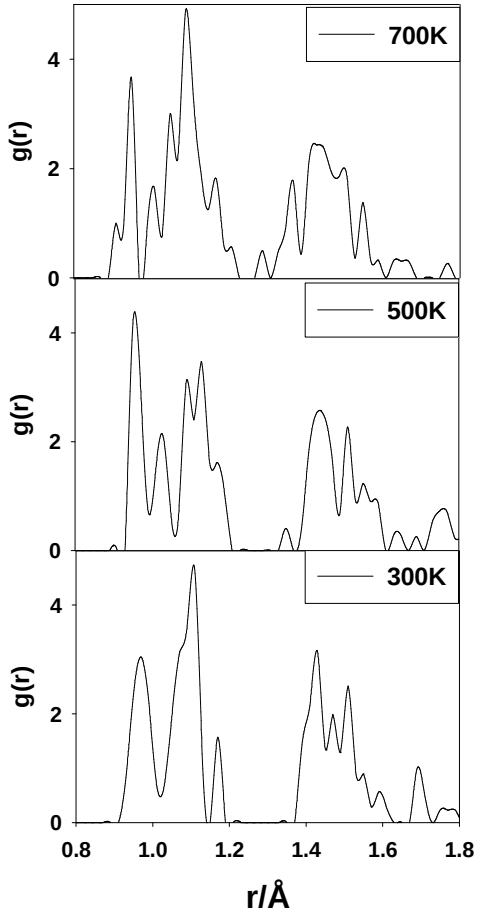

Figure 17. Radial distribution functions for cellulose Iβ at temperatures, 300K, 500K and 700K

radial distances. Also common is that the peaks that were distinguishable in the region 0.9 Å -1.2 Å (C-H, O-H), apparently coalesced when they emerge in the region 1.4 Å -1.6 Å (C-C, C-O). Again, when the temperature is increased, the peaks collapse into a single peak, and this result is predicted in all the structures.

In all the rdf's discussed in this section, there was no much effect on the pair distribution function, g(r) as the temperature was increased. Although it is known that rdf's could signal the melting temperatures of different materials, Sang et al [74] reported that cellulose does not melt before thermal degradation owing to

strong intra and intermolecular hydrogen bonding. The concepts of inter and intra-chain effect was also highlighted, by simulations on gas permeation through siloxane polymer [75]. It was indicated that in order to understand the multitude of peaks it is useful to partition them into intra and inter chain.

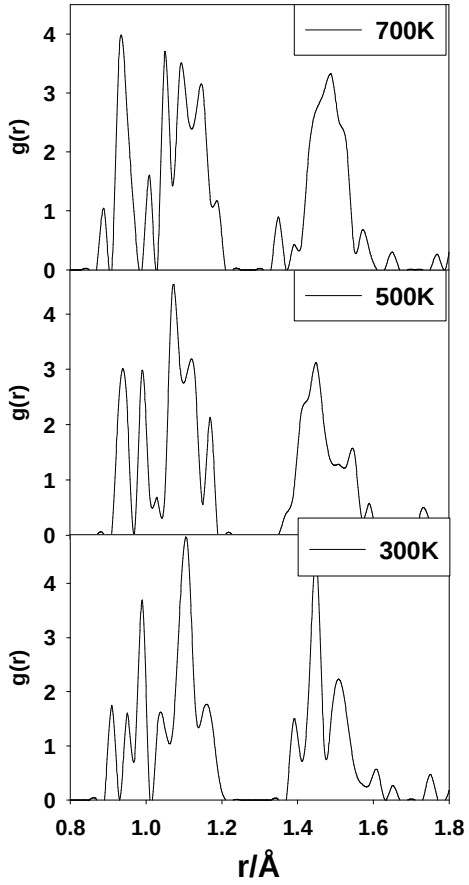

Figure 18. Radial distribution functions for cellulose II at temperatures, 300K 500K and 700K

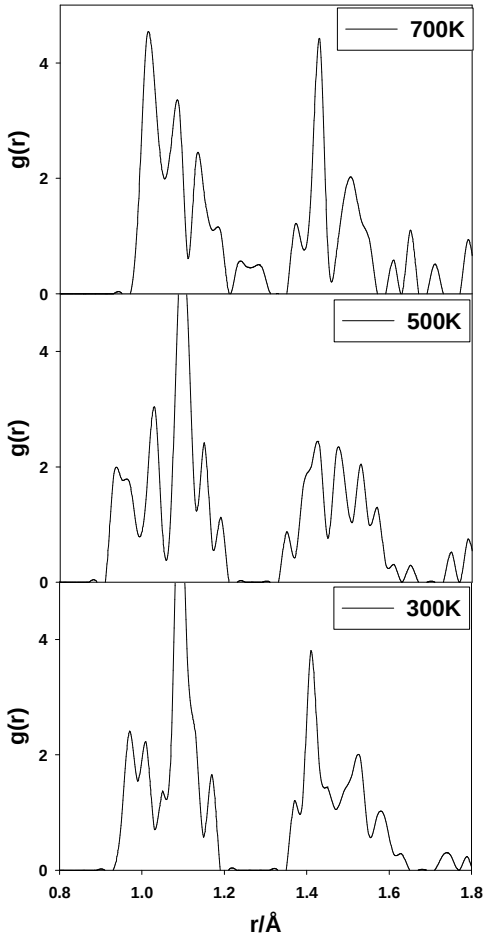

Figure 19. Radial distribution functions for cellulose III at temperatures, 300K 500K and 700K

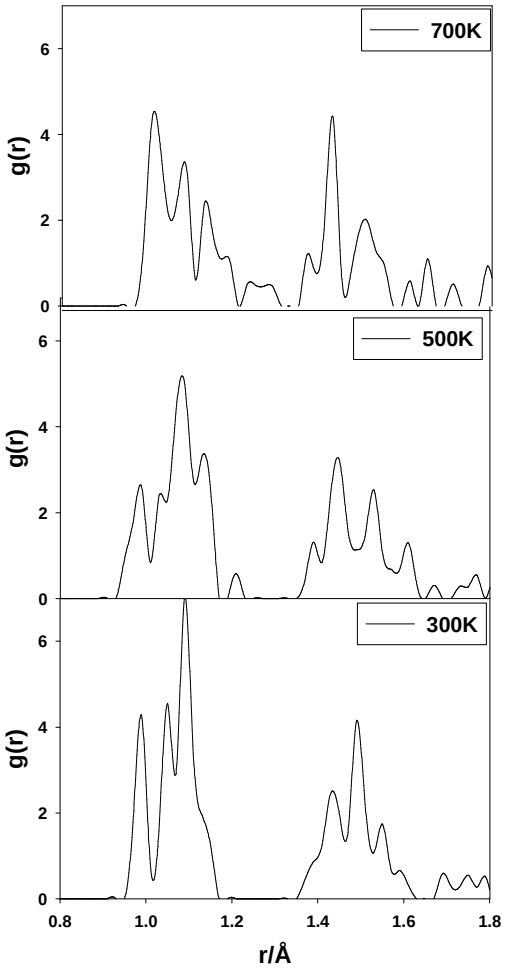

Figure 20. Radial distribution functions for cellulose IV_1 at temperatures, 300K 500K and 700K

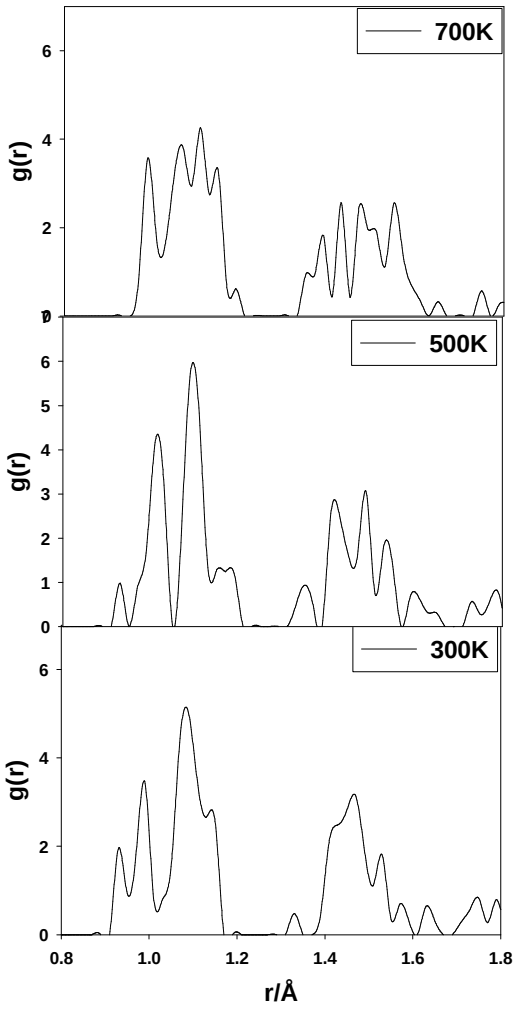

Figure 21. Radial distribution functions for cellulose IV_2 at temperatures, 300K 500K and 700K

3.5 Rdfs calculated at different water concentrations.

In section 3.4, the radial distribution function has shed useful insights on various types of cellulose, at different temperatures. We now perform rdf calculations on cellulose bulk structure with water (at 300K) in order to study the effect of hydration. These calculations were carried out using MD technique employing Discover code in conjunction with the Compass Force Field. Figures 22-26 show the rdf's of cellulose types with and without molecules of water and interestingly, some differences are noted. These rdf calculations were performed at different water concentrations where one and two molecules of water per unit cell were introduced. Generally, broad peaks were observed in the presence of one molecule per unit cell and were not observed when two molecules of water were added.

However, considering cellulose Iβ and cellulose II, figure 22 and 23 respectively, which are the most stable allomorphs, it was found that even after introducing water, the maximum peaks for cellulose Iβ seem to be affected by the presence of water except for the peak position 1.1 Å, which is related to the case where no water was introduced and when one molecule of water was introduced. A sharp peak indicates a state of high crystallinity in the structure. However, regular sharp peaks were observed at almost the same radial distances, and moreover here we noted one common feature that all cellulose types lost long range order earlier than 1.8 Å. This, we ascribed to swelling of the unit cell with increasing number of water molecules, thus reducing the interaction. This, when compared with plots obtained before adding water, we observed that no much deviations were noted.

Also what was noted with cellulose Iβ (figure 22) with addition of two molecules of water was that, the highest sharp peak A´´ was observed at approximately 0.87 Å. Furthermore, one notices peak broadening, B´´(OH) at radial distances around 1.2 Å with addition of two molecules of water. With one molecule of water B´ and

when no water B (OH) was added, we observe that the peak becomes sharper at radial distances approximately 1.15 Å. However in the case of cellulose II, (figure 23) the peaks are occurring at almost the same position, after introducing water, however, one notices peak splitting and coalescing. We observed the coalescing of peaks A_1 and A_2, (corresponding to the dry state) to a peak A´ which reflects a small hump at 1.0 Å. On further addition of water molecule, the peak A´ grows in intensity to A´´. It is obvious that A´´ straddles the 2 A peaks and their centre appears coincident with that of A´´.

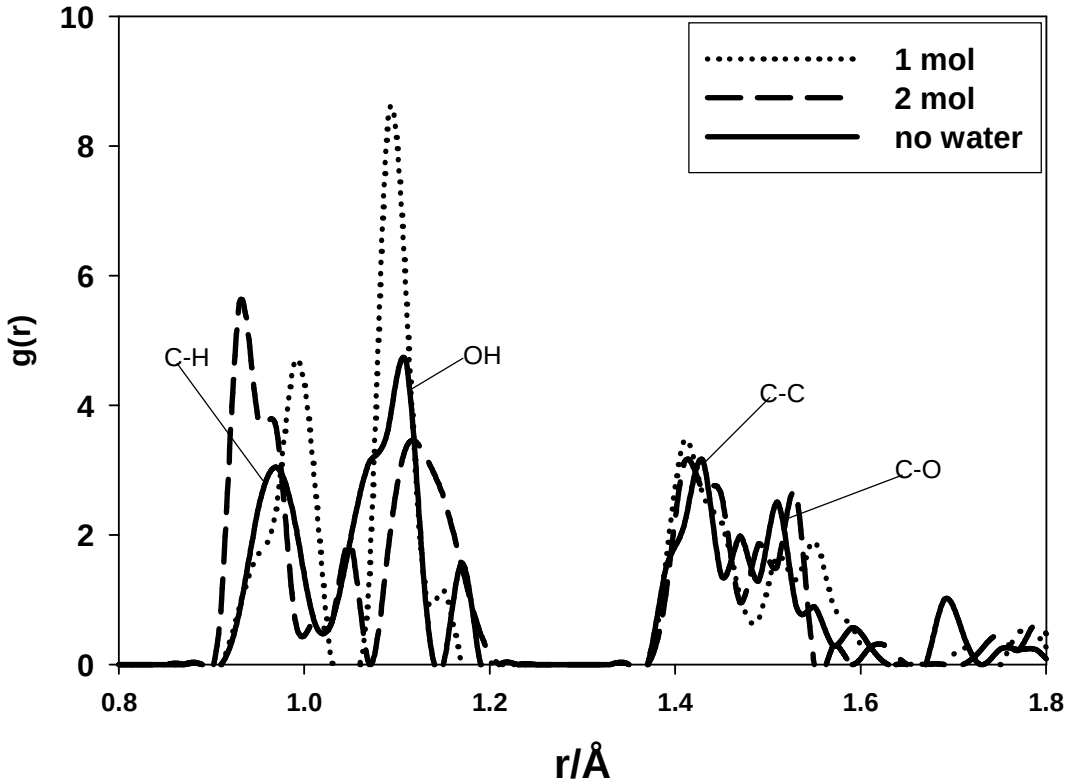

Figure 22. Radial distribution functions for cellulose Iβ with and without water

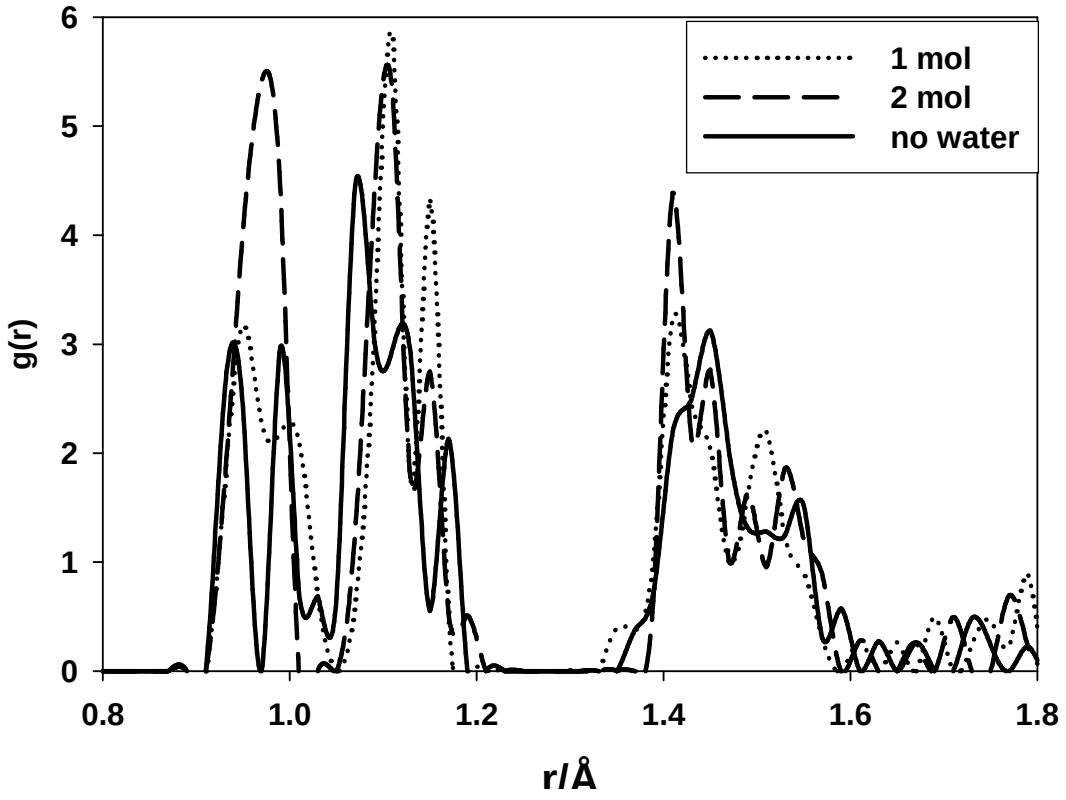

Figure 23. Radial distribution functions for cellulose II with and without water

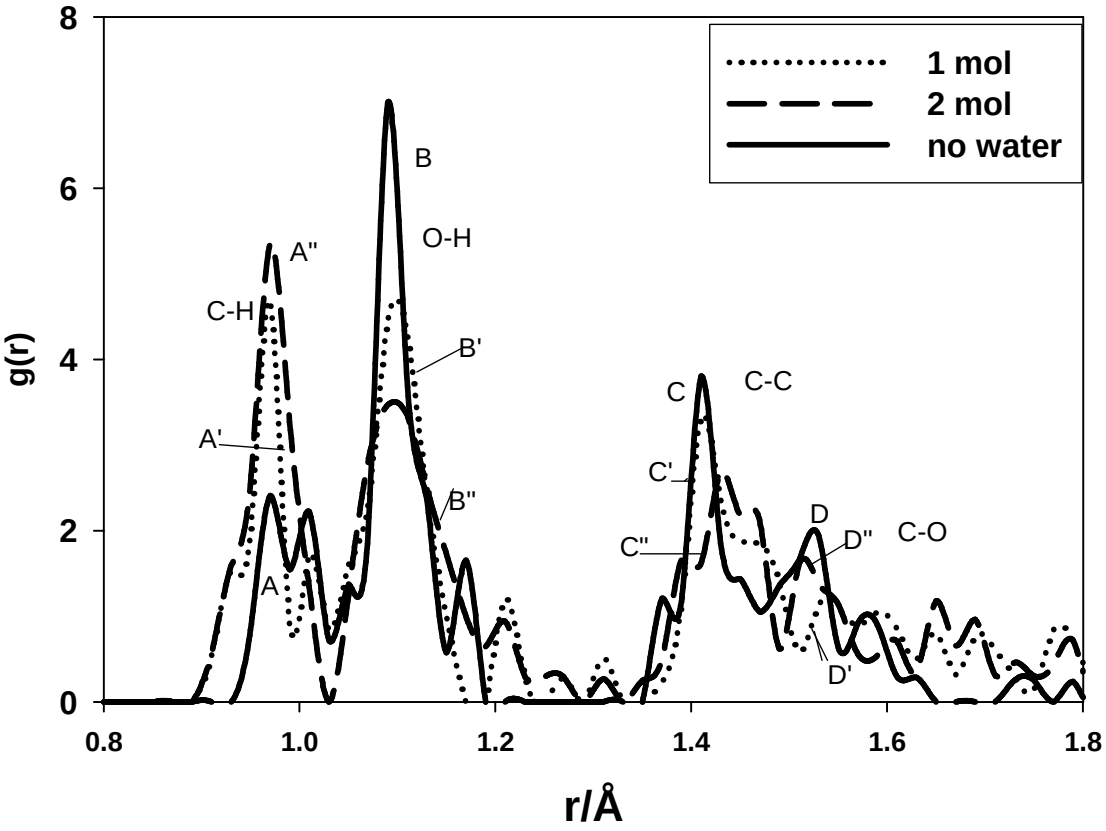

Figure 24. Radial distribution functions for cellulose III with and without water

In figure 24, cellulose III we note that A has grown into A´ and A´ into A´´ with an increase of water concentration. The intensity increases with water concentration (C-H). One also notes the shift of A to the left, and A´ to A´´ when adding water. However, the radial distances of A´ and A´´ were close, indicating a small change with increasing water concentration. Intensities B>B´>B´´, hence reducing with increasing water concentration, especially from one to two molecules of water. The radial distance is almost unaffected (O-H). Intensities C>C´>C´´; C and C´ radial distances are similar with C´´ shifted to the right (C-C). Unlike former groups, intensities D>D´´>D´ (C-O). We notice that radial distance corresponding to D" has shifted while that of D and D´´ are almost similar.

Rdf's of cellulose IV_1, figure 25 depicts intensities A´´>A>A´ and the radial distances for A´ and A´´ are almost similar while that of A has shifted to the

left(C-H). Intensities B>B′>B′′, decrease with increasing water concentration; and the radial distances for B and B′ were unaffected, (O-H) but B′ has shifted. Slightly to the left (C, C′) and C′ (C-C) radial distances are almost similar, while the intensities appear in the order C′′>C′>C, hence increasing with an increase in water concentration. Radial distance of D shift to the right, while D′(C-O) remains unaffected with increasing water concentration. The intensities D>D′>D′′, decreases with increasing water concentration. Figure 26 (cellulose IV_2) shows intensities A<A′<A′′, increasing with increasing water concentration. Also, radial distances, particularly A decreases with increasing concentration of water (C-H), whereas A and A′′ are coincident. The double peak of A coalesce with water addition. Intensities B′′<B′>B, increases with increasing water concentration, and radial distances B′ and B′′ are shifted to the right of B (O-H). Radial distances C′ and C′′ (C-C) are shifted to the left of C while the intensities C′′>C′>C, hence they increase with increasing water concentration and the peaks are sharper. D and D′′ (C-O) radial distances remained unaffected while intensities D′>D~D′′ with the number of water molecules added.

What seemed common to all these allomorphs was that the rdf did not show sharp peaks after 1.6 Å, hence, the structures are not well defined at such radial distances. In comparison, we observed that for a system without water the peaks diminished earlier as opposed to when water was introduced. This trend was noted in all the systems. Very sharp peaks were observed at almost equal radial distances for all allomorphs, and as reported in the previous sections of rdf's. This is indicative of the long range order in the system. The termination observed for pure systems between 1.2-1.38Å for cellulose Iβ, II, III, $IV_1$and IV_2.

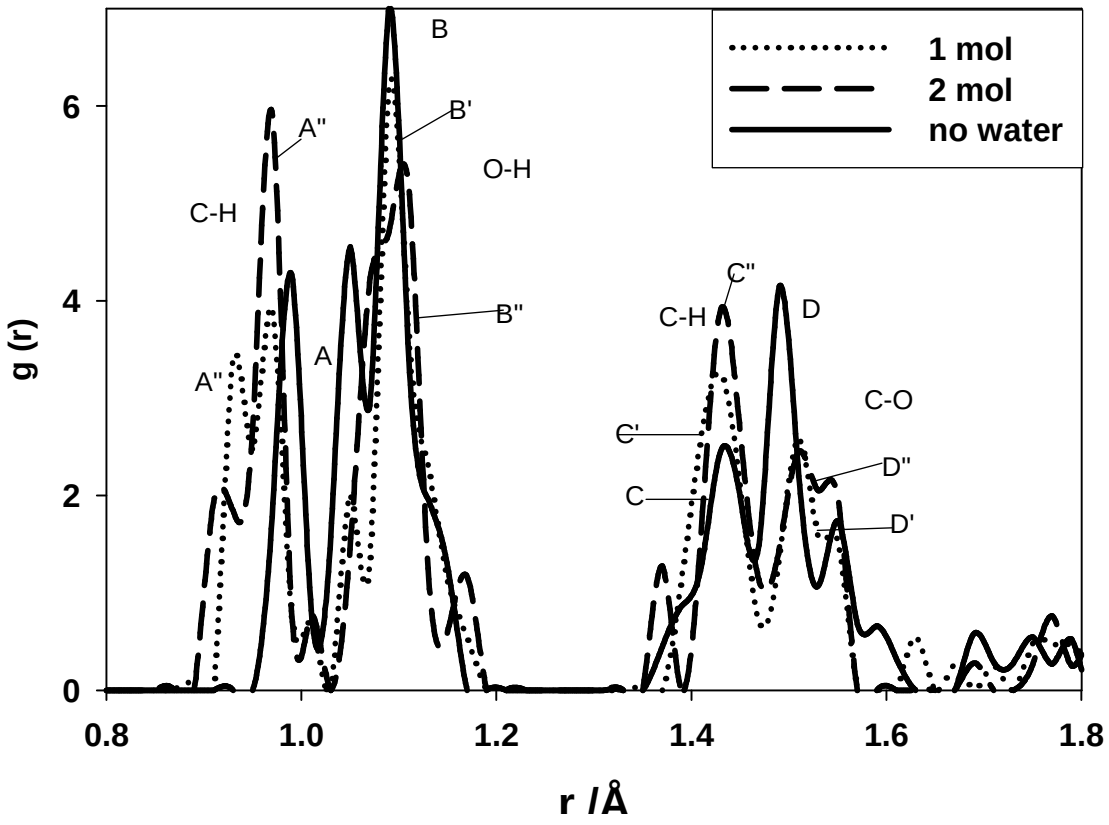

Figure 25. Radial distribution functions for cellulose IV_1 with and without water

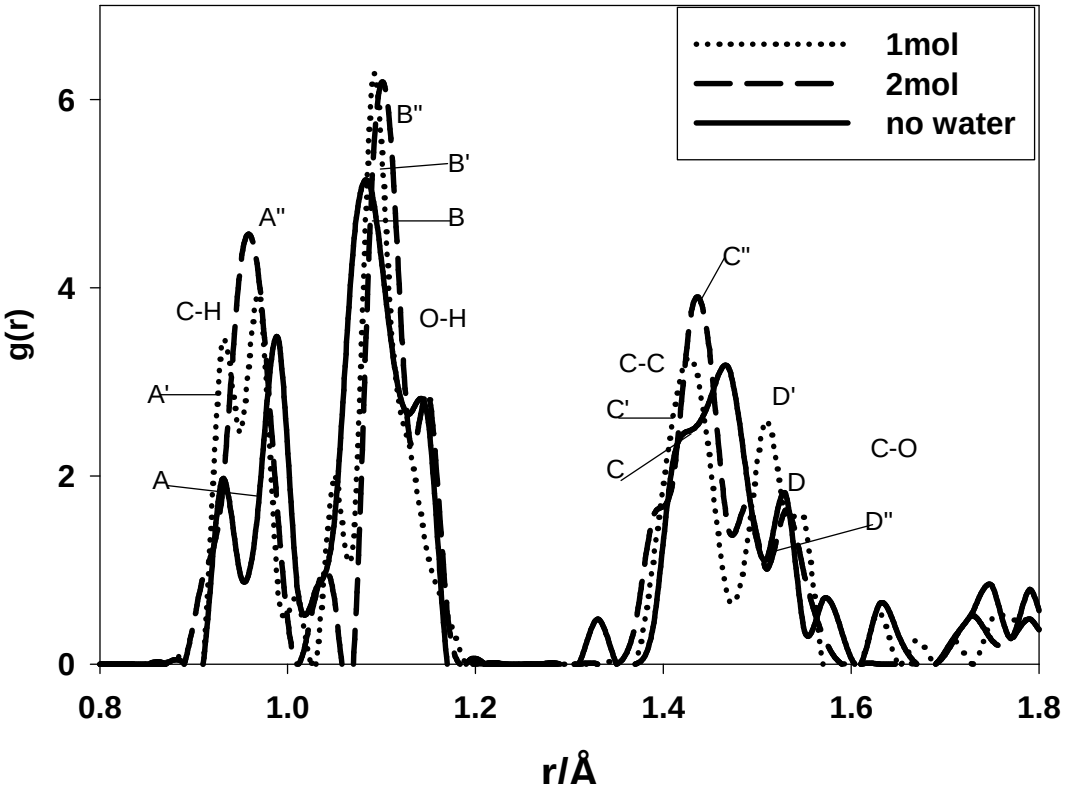

Figure 26. Radial distribution functions for cellulose IV_2 with and without water

3.6 Mechanical properties of cellulose Iβ-IV_2

3.6.1 Introduction

Mechanical properties are usually associated with the extent of bending of bulk materials. These properties help predict a range of ideal elastic moduli for any material type, helping one to design novel crystalline and amorphous polymers, ceramics and semiconductors. Mechanical properties of a polymer are often instrumental in determining its usability. Knowing these properties before synthesis can avoid costly development work invested in polymers that do not exhibit the required mechanical behaviour. In the search for an understanding of the elasticity of natural wood fibers, it is essential to derive theoretical tools to link the structure and mechanical properties of the components into comprehensive composite. We successfully predicted mechanical properties of cellulose Iβ-IV_2 using the formalism explained in section 2.13

3.6.2 Mechanical properties for cellulose Iβ-IV_2 without water

We have calculated mechanical properties of celluloses Iβ-IV_2 at 300K using Discover code as shown in table 12, 13 and 14 respectively. First we calculated these properties for pure systems (table 12) at temperatures 300K, 500K and 600K in order to monitor the effect of temperature on mechanical properties. We found that as the temperature increases, the tensile strength and the shear modulus of cellulose Iβ were decreasing, while that was not the case with other types of cellulose.

We noted that cellulose II gives smaller values of elastic moduli, not comparable with other allomorphs, despite the fact that they all emanate from the same cellulose I, but just differ in the orientation from others. However as indicated in Marhofer et al.[76] that cellulose II shows significantly different physical

properties compared to the raw product, cellulose I, we therefore presume that these and other could be ascribed to the relatively small values of mechanical properties, as in table 12. The smaller Poisson's ratio (300K) for cellulose II could be ascribed to closer intermolecular association through hydrogen bonding and van der Waals forces.

Property (GPa)	Temp. (K)	Iβ	II	III	IV_1	IV_2
Tensile	300	1352.0	151.0	1665.0	1186.0	1109.0
	500	124.6	114.9	1291.0	1044.0	1123.0
	600	121.5	24.44	1119.0	932.9	930.1
Poisson's ratio, ν	300	0.2618	0.0762	0.1027	0.1326	0.2121
	500	0.2034	0.4545	0.2731	0.2908	0.1884
	600	0.3457	0.0478	0.2850	0.2440	0.2746
Bulk Modulus, K	300	945.6	59.4	698.4	537.9	641.7
	500	70.00	89.53	821.6	743.2	600.7
	600	131.3	42.37	1001.0	679.8	687.6
Shear Modulus, G	300	535.6	70.1	754.9	523.4	457.3
	500	51.75	8.404	439.4	361.4	472.6
	600	45.15	58.84	502.5	419.6	364.9

Table 12 . Compass force field mechanical properties for pure systems at different temperatures

Property, GPa	Iβ	II	III	IV_1	IV_2
Tensile	71.84	65.52	45.94	68.69	65.94
Poisson's ratio, ν	0.0976	0.1155	0.1187	0.0880	0.1267
Bulk Modulus, K	29.75	28.40	20.08	27.79	29.44
Shear Modulus, G	32.72	29.37	20.54	31.56	29.26

Table 13 . PCFF mechanical properties for celluloses (Iβ-IV_2) at 300K

The authors [76] further reported on computer simulations of crystal structures and elastic properties of cellulose and concluded from these results that cellulose II, as resulting from the mercerization, is arranged in parallel chains. Microscopically the transition from phase I to II can then easily be explained as a rearrangement of the exocyclic torsional angles; hence we presumed that these and other factors could be the contributing factors in the behaviour depicted in table 12 and 13. Richard et al [77] further reported the calculated Young's modulus of cellulose Iβ as 148 GPa and that of cellulose II as 168 GPa.

However, further calculations using PCFF (table 13) have shown that mechanical properties for pure systems in all the celluloses compare reasonably well with each other as compared to those obtained using Compass force field (table 12). The Poisson's ratio for all allomorphs was around 0.1. The bulk modulus and shear modulus for cellulose III was found to be approximately 30 GPa, except for cellulose III, which gave a value of 20.08 GPa and 20.54 GPa, respectively. Bledzki [51] further reported the tensile strengths of sisal, flax and glass fibre as 38 MPa and 55 MPa for sisal, 47 MPa and 67 MPa for flax and 100 MPa for glass. Figures 3.12 and 3.13 give the bulk modulus and the tensile strength against temperatures for all types of cellulose. We notice that these two elastic properties

are neither increasing nor decreasing with temperature. However, Heiner et al [73] reported the tensile strength of the Iα and Iβ along the chain as 135 GPa and the pressure along **a** and **b** were -0.42 and -0.74 GPa respectively. However, we observed that the tensile strength for Iβ obtained at 300K is much higher than the one observed by Richard et al [77]. For cellulose II, a good correlation was observed. Comparing the two force fields and especially cellulose II, the tensile strength predicted with PCFF is almost double that which was observed using Compass force field.

Heiner et al further highlighted that experimentally, the tensile strengths of these axes are not known. However, Kroon-Batenburg et al [78] estimated the tensile strength due to the intramolecular hydrogen bonds to be approximately 65GPa. However, Chen et al [79] in their work on cellulose I and II reported the bulk moduli, shear moduli and Poisson's ratio of these celluloses as 13,258 $\pm$ 1.731, 5.955 $\pm$ 0.673 and 0.232 $\pm$ 0.0313, respectively. These values did not very well compare with our results.

Bledzki et al, reported Young's modulus of cellulose I and II, and indicated that mechanical properties of natural fibres depend on its cellulose type, since each cellulose has its own cell geometry and the geometrical conditions determine the mechanical properties. Their experimental values were reported as 74-103 GPa (Flax, hemp), 110 GPa (Flax), 130 GPa (Ramie), 120-135 GPa (Ramie) for cellulose I. Their calculated values were 136 GPa and 168 GPa for cellulose I and 89 GPa and 162 GPa for cellulose II. However, their results did not explain one order of magnitude as opposed to our results. From table 12, with reference to 300K, it was noted that cellulose II had properties with values one order of magnitude lower than other systems.

Compass force field results, particularly for the Iβ cellulose at 300K, are an order of magnitude higher than values cited in some literature. In order to further verify these values, preliminary ab initio calculations were performed and mechanical properties of cellulose Iβ types were calculated, without optimising atomic positions owing to limited computational resources. In these calculations, the bulk, shear, and Young's moduli were obtained as 133.3 GPa, 128.9 GPa and 292.4 GPa, respectively. Hence, we note that the moduli of Cellulose Iβ at higher temperatures (table 12), determined with Compass force field, compare better with PCFF results (table 13).

Figures 27 and 28 show the variation of tensile strengths and bulk moduli of cellulose polymorphs with temperature respectively; where three regions of interest are generally noted. In the first region (300 – 400K), the tensile strength is near constant for cellulose II and IV_1, decreases for cellulose Iβ and IV_2 and increases for cellulose III. Tensile strengths of all cellulose polymorphs reduce (with Iβ decreasing significantly) in the second temperature region, ranging from 400 to 500K; and finally gradually increase in the third region beyond 500K.

Temperature variation of bulk moduli of the cellulose polymorphs in the three temperature regions are depicted in Figure 28. We note an increase for cellulose III, IV_1 and $1V_2$ a reduction for Iβ and a near constant behaviour for II, in the first region 300K- 400K. In the second region (400-500K), the bulk moduli of cellulose Iβ, III and IV_2 reduce with the former experiencing a steepest decrease, and those of cellulose II and IV_1 tend to a constant value. As for the third region, above 500K, bulk moduli of cellulose Iβ, III and IV_2 are reversed and begin to increase while those of II and IV_1 reduce slightly.

It is quite explicit that mechanical properties of the allomorphs change in the three identified temperature regions. Whilst a direct explanation of changes noted in the

first and second region is not readily available, the anomalous features noted in the third region (above 500K) can be associated with the burning of cellulose polymorphs, since their ignition temperature is experimentally reported as 506K [77]. It is therefore encouraging to note that predictions from simulations are sensitive to experimentally observed phenomena.

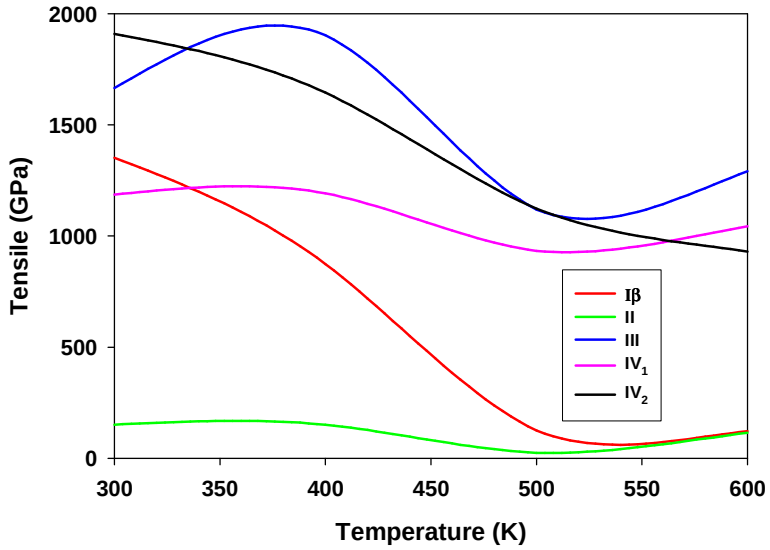

Figure 27. The change of tensile strength with temperature of different cellulose types

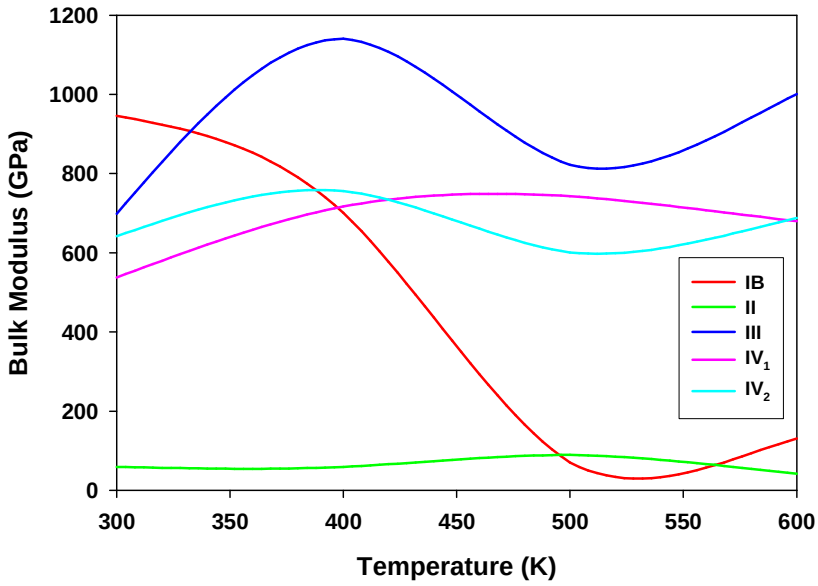

Figure 28. The change of bulk modulus with temperature of different cellulose types

3.6.3 Mechanical properties for cellulose Iβ-IV_2 with water

We further calculated mechanical properties of cellulose with water (see table 14) at 300K using Compass Force Field. For pure systems, table 12, 300K, it was observed that for cellulose II, the tensile strength, shear, bulk and Poisson's ratio were not comparable with other cellulose types. Table 14, clearly shows that the values decrease with an increase in the number of water molecules, hence a decrease in the elasticity.

This behaviour was clearly observed for the tensile strength, bulk moduli and shear moduli of celluloses Iβ, II, III, IV_1 and IV_2. However, cellulose Iβ shows an increase in values of bulk and shear modulus, from one to two molecules of water consecutively. Cellulose III and IV_2 also shows an increase in values of Poisson's ratio with the change from one to two molecules of water. Table 14 again depicts

that as the water concentration increases the values of tensile strength, bulk modulus and the shear modulus are decreasing, except for cellulose Iβ. More insight into the trends depicted by mechanical properties of various cellulose types as water was introduced, was further shown in figures 29-33. In these figures, we have shown how tensile strength, bulk moduli and shear moduli of celluloses Iβ, II, III, IV_1 and IV_2 vary with changing water concentration.

Cellulose					
	Iβ	II	III	IV_1	IV_2
Tensile Strength					
1 H_2O molecule	27.59	47.10	40.94	45.52	36.06
2 H_2O molecules	41.87	33.39	22.09	28.55	16.27
Poisson's ratio, ν					
1 H_2O molecule	0.1810	0.1823	0.2176	0.1250	0.1752
2 H_2O molecules	0.1032	0.1650	0.2390	0.1120	0.2990
Bulk Modulus, K					
1 H_2O molecule	14.41	24.71	24.16	20.23	18.50
2 H_2O molecules	17.58	16.61	14.11	12.26	13.49
Shear Modulus, G					
1 H_2O molecule	11.68	19.92	16.81	20.23	15.34
2 H_2O molecules	18.98	14.33	8.914	12.84	6.261

Table 14. Calculated mechanical properties after wetting at 300K

It was noted also for celluloses Iβ and IV_2 that before water was introduced, the bulk moduli were greater that the shear strength, except for cellulose IV_1 where the bulk modulus and tensile strength were almost identical. Celluloses II and III, the shear

modulus was greater than bulk modulus before adding water. However, this behaviour was not observed for other celluloses.

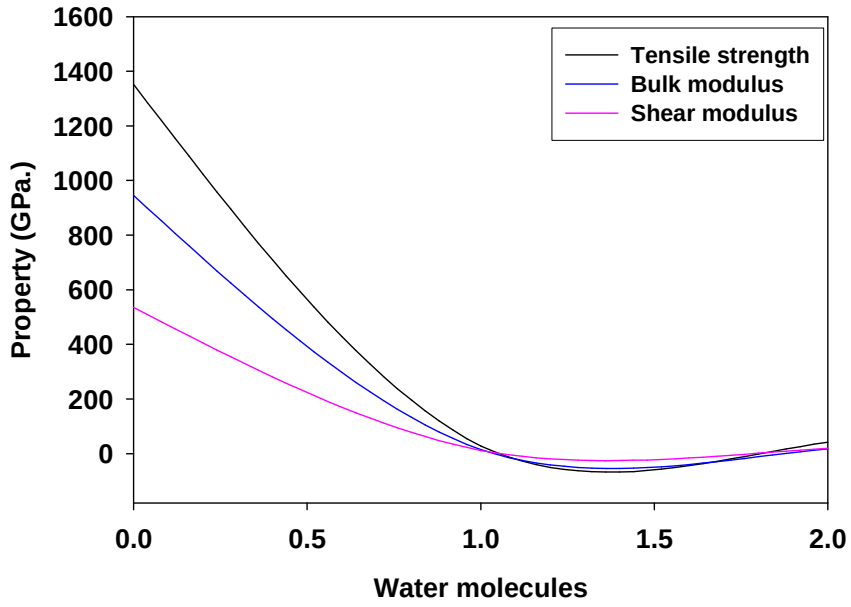

Figure 29 The change of mechanical properties with increasing water concentration of cellulose Iβ

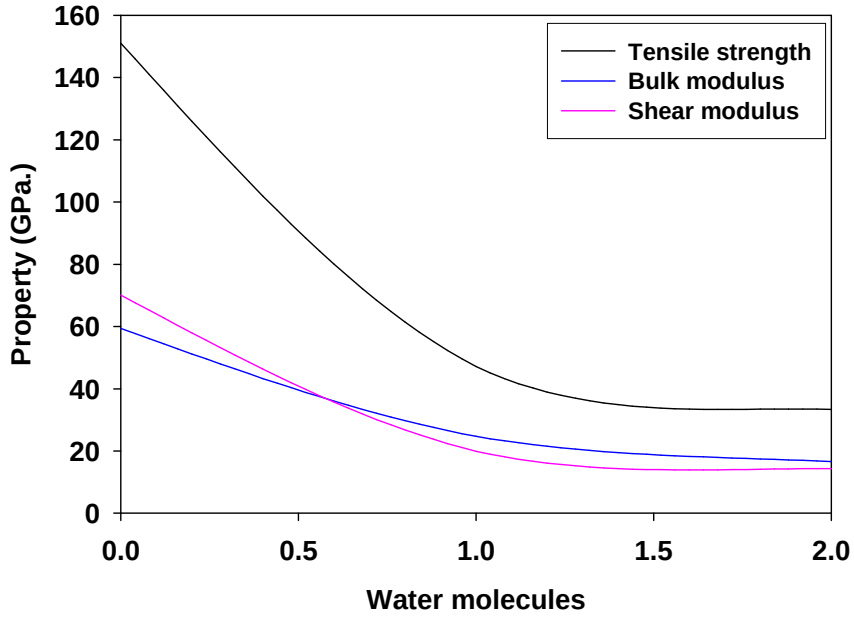

Figure 30 The change of mechanical properties with increasing water concentration of cellulose II

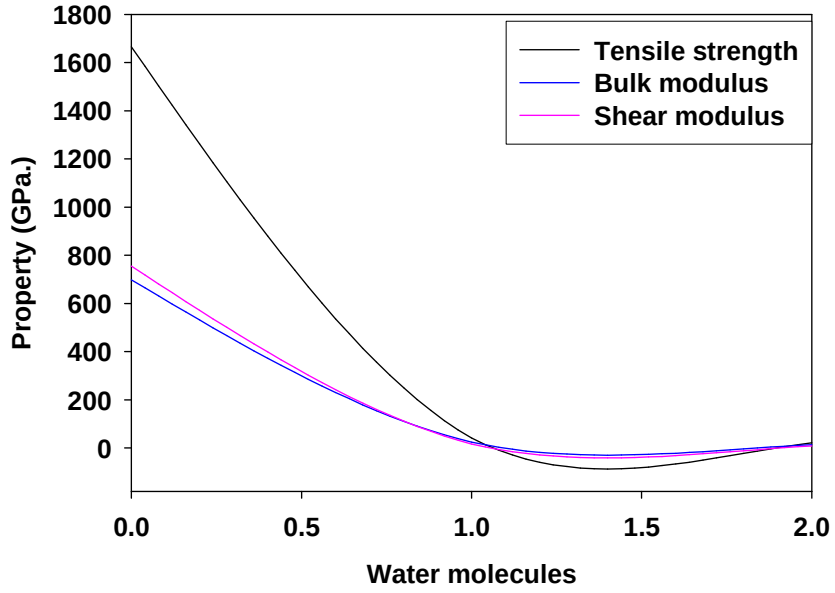

Figure 31. The change of mechanical properties with increasing water concentration of cellulose III

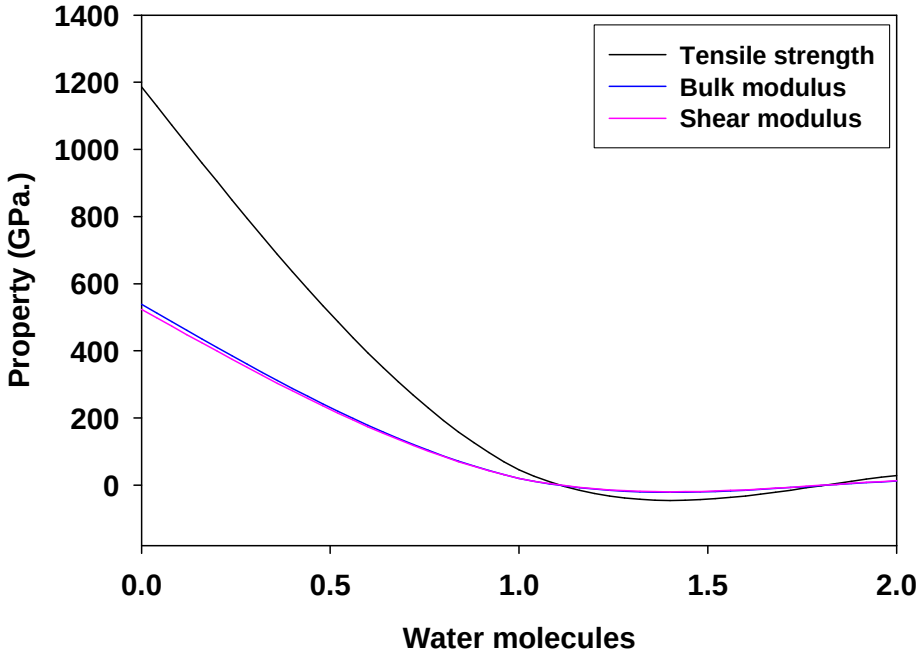

Figure 32. The change of mechanical properties with increasing water concentration of cellulose IV_1

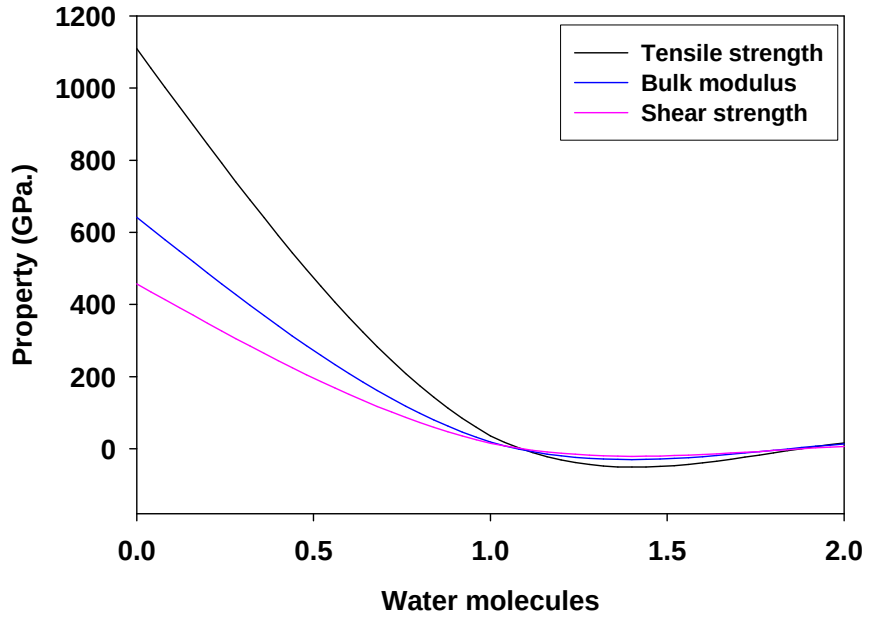

Figure 33. The change of mechanical properties with increasing water concentration of cellulose IV_2

The Poisson's ratio of various celluloses at various water concentrations is given in figure 34, and it can be said that this property did not show major changes before introducing water and this behaviour was noted in all the systems. Cellulose Iβ and IV_1 were both decreasing linearly with increasing water content, but Iβ was initially higher than that of IV_1 and the opposite was observed after addition of one molecule of water. Poisson's ratio of cellulose II and III increased with the introduction of the second molecule of water. Also what appears clear is that cellulose IV_2 was decreasing until one molecule of water was added after which it increased.

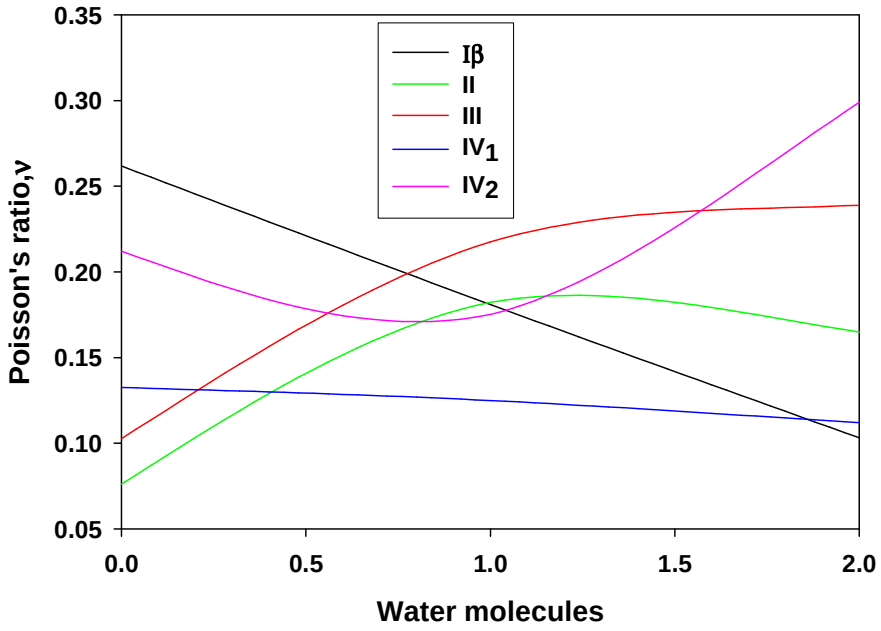

Figure 34. The change of Poisson's ratios of various celluloses with increasing water concentration

Chapter 4

4 Conclusion and Recommendations

4.1 Conclusion

We have presented simulation results on structural and mechanical properties of five cellulose allomorphs, namely cellulose Iβ, II, III, IV_1 and IV_2. Molecular dynamics simulation technique, using Compass force field, has been employed in the study. PCFF was also used in calculations of lattice parameters and mechanical properties, for comparison with Compass results. Generally, Compass Force Field proved to have reasonably reproduced the structural properties of cellulose allomorphs, thus, this justifies why this force field was invoked in generating most of the results in this work.

Predicted lattice parameters are in close agreement with experimental evidence, for both minimization and MD results. Meanwhile, we observed that lattice parameters calculated with both Compass and PCFF did not very well reproduce experimental observations, Compass force field results are systematic. The interactions of cellulose with water have been studied and lattice parameters as well as mechanical properties were calculated for all five allomorphs. Cell volumes showed an increase with water concentration, which is indicative of swelling in the cellulose. Calculations of lattice parameters at various pressures were conducted and it was noted that as the pressure increases the lattice parameters decrease which showed compression of the cell parameters. Dihedral angles for the $^4C_1$ were also calculated and agreed favorably with the results found on similar polysaccharides.

We have calculated the radial distribution functions (rdf's) at various temperatures, which have very well described our systems. Rdf's for systems with water were also calculated and almost similar characteristics for all the allomorphs in terms of radial distances were noted, signalling the originality of the allomorphs.

Mechanical properties were calculated for structures with and without water, using Compass force field, and the results were not comparable for all allomorphs, particularly cellulose II which differed from the rest by one order of magnitude. However, further calculations using PCFF did not reflect anomalous elastic moduli of cellulose II. However, there were orders of magnitude different from those of Compass. The introduction of water molecules has seen the tensile strength, bulk modulus and the shear modulus decrease, with the exception of cellulose Iβ. Lastly, the bulk modulus and tensile strength were graphically presented at different temperatures and from these, it was observed that at higher temperatures, there was a decrease in the values of mechanical properties up to about 500K, after-which a gentle increase was observed. Interestingly, 500K is the ignition temperature of the cellulose structures.

4.2 Recommended future work

Bulk structural and mechanical properties of cellulose allomorphs have been studied using MD simulation technique. However, we would like to put forward some recommendations emanating from the current study. The work that has been done on the structural as well as mechanical properties of these materials can serve as a good basis for further studies on the systems. These will include calculations of diffusion coefficients on larger systems; supercells and also on the composites involving the interaction of the fiber with the matrix. In this case $CaCO_3$ and TiO_2 could serve as good candidates. Bulk structural properties of cellulose fibers have been studied extensively using force fields methods. Little work has been done on these series of fiber properties, thus we recommend that further intense

measurements should be carried out by experimentalists and be compared with our current calculations. Mechanical properties of these allomorphs will be of great interest, as such properties are known to impact positively in the decision made when using these materials and in further calculations. In this work, we managed to predict a wide range of structural and mechanical properties, which need to be confirmed by experiments.

Computer simulations proved to be a successful tool for studying cellulose fibers since it gives a key understanding on the structural and elastic properties of the systems studied in this work. We thus recommend further work on these properties. It is hoped that the work done thus far will lay a foundation for a better understanding of cellulose allomorphs. It is necessary, however, that a good force field be developed first.

Bibliography

[1] T. Kondo, in `Polysaccharides, Structural Diversity and Functional Versatility', Ed. S Dumutriu, Marcel Dekker Inc, New York 1998, 11

[2] G. Meshitsuka, A. Isogai, in `Chemical Modification of Lignocellulosic Materials', Ed. D.N.S. Hon, Marcel Dekker Inc, New York 1996, 11

[3] T. Imai, J. Sugiyama, T. Itoh and F. Horie, J. Struct. Biol. 1999, **127**, 248

[4] J. Sugiyama, T. Okano, H. Yamamoto and F. Horie, Macromolecules 1990, **23**, 3196

[5] J. Gassan, Composites Part A 2002, **33,** 369.

[6] J. Gassan, Composites Part A 2002, **33,** 369

[7] W. Chen, G.C. Lickefield and C.Q. Yang. Polymer 2004, **45,** 77

[8] W. Chen, G.C. Lickfield and C.Q. Yang. Polymer 2004, **45,** 1063

[9] E.M. Debzi, H. Chanzy, J. Sugiyama, P. Tekely and G. Excoffier, Macromolecules 1991, **24**, 6816

[10] J. Schurz, Prog. Polym. Sci. 1999, **24**, 481

[11] http://www.Fibersource.com/f-tutor/cellulose.htm

[12] K.H. Gardner and J. Blackwell. Biopolymers 1974, **13**, 1975

[13] A. Sarko and R. Muggli, Macromolecules 1974, **7**, 486

[14] K. H. Gardner and J. Blackwell, Biopolymers 1974, **13**, 1975

[15] A. Stipanovic and A. Sarko, Macromolecules 1976, **9**, 851

[16] S. W. Nam, Dept. Of Chemical and Biomolecular Eng, University of Murrayland, College Park, MD 20742-2111

[17] J. Ayashi, A. Sufoka, J. Ohkita, and S. Watanabe, Polym. Lett. 1975, **13**, 23

[18] J. Sugiyama, J. Persson and H. Chanzy, Macromolecules 1991, **24**, 2461,

[19] A. Vasella, Pure and Appl. Chem. 1998, **70**, 425

[20] G. Meshitsuka and A. Isogai, in Chemical modification of lignocellulosic materials, Ed D N. S. Hon. Marcel Dekker Inc. New York 1996, 11

[21] J. Sugiyama, R. Vuong and H. Chanzy, Macromlolecules 1991, **24**, 4168

[22] P. Zugenmaier , Prog. Polym. Sci. 2001, **26,** 1341

[23] V.L. Finkenstadt and R.P. Millane, Macromolecules 1998, **31**, 3776

[24] F.J. Kolpak and J. Blackwell. Macromolecules 1976, **9**, 273

[25] A.J. Stipanovic and A. Sarko. Macromolecules 1976, **9**, 851

[26] A.Sarko and R. Muggli, Macromolecules 1974, **7**, 486

[27] J. Hayashi, A. Sufoka, J. Ohkita and S. Watanabe, Polym. Lett. 1975, **13,** 23

[28] A. Sarko, J. Southwick and J. Hayashi. Macromolecules 1976, **9,** 857

[29] F. J. Kolpak and J. Blackwell, Macromolecules 1975, **8**, 563

[30] E.S. Gardiner and A. Sarko, Can. J. Chem. 1985, **63**, 173

[31] H. Chanzy, B. Henrissat, M. Vincendon, S.F. Tanner and P. Belton, Carbohydr. Res. 1987, **1,** 160

[32] R. H. Marchessault and A. Sarko, Adv. Carbohydr. Chem. 1967, **22**, 421

[33] S. W. Nam, Dept. Of Chemical and Biomolecular Eng, University of

[34] M. Inder, T. Saxena, R. Dandekar and M. Brown Jr., Cellulose Biosynthesis: Current views and evolving concepts, Section of Molecular Genetics and Microbiology, School of Biological Sciences, The University of Texas at Austin, Austin, TX 78712, USA, 2005

[35] A. Bergander, Local variability in chemical and physical spruce wood fibers, Doctoral thesis, 2001

[36] J. Gassan and A.K. Bledzki. 7th Internationals Techtexil Symposium Frankfurt, 20-22 June 1995

[37] A.R. Sanadi, D. F. Caufield and R. M. Rowel, Plastic Eng. 1994, **27**, 4

[38] E.J.W. Barber, Prehistoric Textiles, Princeton University Press, Princeton, NJ, USA, 1991, 12

[39] (a) H.J.J. Wellard, Polym. Sci. 1954, **23**, 471. (b) H.J. Marrinan, J. Mann, Ibib. 1956, **21**,301

[40] D. W. Jones, "Cellulose and Cellulose derivatives", N.M. Bikales, L. Segal, Eds. Wiley-Interscience: New York, Part IV 1971, 117

[41] O. Ellefson and B.A. Tonnesen, “Cellulose and Cellulose derivatives"; N.M. Bikales, L. Segal, Eds. Wiley Interscience: New York, Part IV 1971,151

[42] A.D. French, Carbohydr. Res. 1978, **61**, 67

[43] C. Clemens, Exploratory Microscopic Investigation of Impacted Paper Fiber-reinforced Polypropylene Composites, http://www.rmmn.org/documnts/pdf1995/clemo95a.pdf.

[44] J. Sugiyama, R. Vuong and H. Chanzy, Macromolecules 1991, **24**, 4168

[45] H. M. Meyer and K. H. Ber. Dtsch. Chem. Ges. 1928, **61B**, 593

[46] K.H.Meyer and L. Misch, Helv. Chim. Acta 1937, **11**,534

[47] Y. Rabin, J. Chem. Phys. 1987, **86**, 5215

[48] J.R. Marhofer, S. Reiling and J. Brickmann, J. Phys. Chem. 1996,**100,** 1350

[49] R.R. Maphanga, Computational Modelling and EXAFS Studies of Electrolytic Manganese Dioxide, PhD Thesis, 2005

[50] http://www.accelrys.com

[51] B.J. Alder and T.E. Wainwright, J. Chem. Phys. 1957, **27**, 1208

[52] B.J. Alder and T.E. Wainwright, J. Chem. Phys.1959, **31**, 459

[53] A. Rahman, Phys. Rev. 1964, **136**, 405

[54] J.A. Young, B.L. Farmer, and J.A. Hinkley, Polymer 1999, **40**, 2787

[55] D. Rigby, Phase Equilibria 2004, **217**, 77

[56] L. Verlet, Phys. Rev. 1968, **165**, 201

[57] M. P. Allen and D. J. Tildesley, Computer Simulations of Liquids. Clarendon, Oxford, 1987

[58] A. Nakano, "Class notes for CSCI 599: High performance scientific computing", University of Southern, California, Fall Semester, 2003

[59] R.W. Hockney and J.W. Eastwood, Computer Simulation Using Particles {McGraw-Hill}, New York, 1988

[60] L. Verlet, Phys. Rev. 1967, **159**, 98

[61] E. Wimmer, J. Mat. Sci. and Eng. 1996, **B37,** 72

[62] N. S. Wang, "Cellulose degradation". Department of Chemical Engineering, University of Maryland College Park, MD 2074-2111

[63] (a) A.T. Hagler, E. Dauber, S. Lifson, J. Am. Chem. Soc. 1979, **101**, 5122

(b) A.T. Hagler, P. Dauber, S. Lifson, J. Am. Chem. Soc. 1979, **101**, 5131

[64] D. Rigby, Phase Equilibria 2004, **217**, 77

[65] L. Verlet, Phys. Rev. 1968, **165**, 201

[66] http://www.accelrys.com/products/datasheets/discover.pdf

[67] A.R. Leach, Molecular Modelling principles and Applications; Glaxo Wellcome Research and Development and the University of Southampton, 1999

[68] M.S. Islam., M. Cherry and C.R.A. Catlow, J. Solid State Chem. 1996, **124,** 230

[69] M.A. Mahladisa, Molecular dynamics simulations of bulk and {100} surface properties of Gold at different temperatures using the Sutton-Chen Potentials, MSc. Thesis, 2004

[70] K. J. Naidoo and J.W. Brady, J. Chem. Phys. 1997, **224,** 263

[71] L.M.J Kroon-Batenburg, B Bouma, and J. Kroon, Macromolecules 1996, **29**, 5695-5699, Stability of cellulose structures studied by MD simulations. Could Mercerized cellulose II be parallel?

[72] Z. Yao, C. C. Zhu, M. Chen and J. Liu, *Comp. Mat. Sci.* 22, 180 (2001)

[73] A P. Heiner, J. Sugiyama and O. Teleman, Crystalline Cellulose 1-alpha

[74] Sang Youn Oh, Dong II Yoo, Younsook Shin and Gon Seo: FTIR analysis of cellulose treated with sodium hydroxide and carbon dioxide, 417-428, 2005

[75] L.R.M Segooa, Investigation of Gas Permeation through Siloxane Polymer by Molecular dynamics, MSc. Thesis, 2000

[76] J.R. Marhöfer, S. Reiling, and J. Brickmann *Ber. Bunsenges.* J. *Phys. Chem.* 1996, **100**, 1350

[77] J Richard. Marhöfer, Stephan Reiling, and Jürgen Brickmann *Ber. Bunsenges.* Computer Simulations of Crystal Structures and Elastic Properties of Cellulose, *Phys. Chem.* **100**, 1350 (1996).

[78] A. Amash and P. Zugenmaier: Polymer 2000, **41,** 1689

[79] H. L. Chen and R. G. Porter, J. Appl. Pol. Sci. 1994, **54**, 1781

Appendix A

Papers presented at conferences

1. M.G. Mashapa et al, “Modelling studies of the structure and properties of cellulose fibres, " Presented at Interscience Conference, University of Limpopo, Turfloop Campus, Sovenga (SA), in October 2003.
2. M.G. Mashapa et al, "Modelling Studies of the structure and properties of cellulose fibres," Presented at South African Institute of Physics (SAIP) Annual Conference, held at University of Stellenbosch, in June 2003
3. M.G. Mashapa et al., " Structure and properties of cellulose Fibres: Computer Simulation study," Presented at the Eighth Annual Materials Modelling Meeting, held at University of Limpopo, Turfloop Campus, Materials Modelling Centre, Sovenga (SA), in March 2004.
4. M.G. Mashapa et al, “Structure and properties of Crystalline cellulose Fibres," Presented at South African Institute of Physics (SAIP) Annual Conference, held at University of the Free State, in June 2004
5. M.G. Mashapa et al., “Structural properties of cellulose Fibres, Computer simulation study," Presented at the Ninth Annual Materials Modelling Meeting, held at University of Limpopo, Turfloop Campus, Materials Modelling Centre, Sovenga (SA), in March 2005.
6. M.G. Mashapa et al., “Structural properties of cellulose Fibres, Computer simulation study," Presented at South African Institute of Physics (SAIP) Annual Conference, held at University of Pretoria, in July 2005

Appendix B

Fractional coordinates of celluloses studied

Table A.
Fractional coordinates of cellulose Iβ. Monoclinic unit cell, space group $P2_1$ a = 7.85 Å, b = 8.27 Å, c(fiber axis) = 10.38 Å, γ = 96.3°. Parallel chains.

Chain 1 (corner):			
Atoms	x	y	z
C11	0.0078	-0.0430	0.0457
C21	-0.0415	-0.1803	-0.0497
C31	0.0365	-0.1346	-0.1806
C41	-0.0185	0.0275	-0.2248
C51	0.0196	0.1569	-0.1210
C61	-0.0528	0.3145	-0.1531
O21	0.0155	-0.3264	-0.0022
O31	-0.0182	-0.2586	-0.2722
O41	0.0733	0.0827	-0.3379
O51	-0.0545	0.1025	0.0000
O61	0.0443	0.4037	-0.2511
H11	0.1482	-0.0233	0.0547
H21	-0.1820	-0.2011	-0.0575
H31	0.1771	-0.1253	-0.1738
H41	-0.1566	0.0109	-0.2458
H51	0.1592	0.1838	-0.1093
H61A	-0.1872	0.2879	-0.1834
H61B	-0.0563	0.3887	-0.0654
C12	-0.0078	0.0430	0.5457
C22	0.0415	0.1803	0.4503
C32	-0.0365	0.1346	0.3194
C42	0.0185	-0.0275	0.2752
C52	-0.0196	-0.1569	0.3790
C62	0.0528	-0.3145	0.3469
O22	-0.0155	0.3264	0.4978
O32	0.0182	0.2586	0.2278
O42	-0.0733	-0.0827	0.1621
O52	0.0545	-0.1025	0.5000
O62	-0.0443	-0.4037	0.2489
H12	-0.1482	0.0233	0.5547
H22	0.1820	0.2011	0.4425
H32	-0.1771	0.1253	0.3262
H42	0.1566	-0.0109	0.2542
H52	-0.1592	-0.1838	0.3907
H62A	0.1872	-0.2879	0.3166
H62B	0.0563	-0.3887	0.4346

(Chain 2 (center)			
Atoms	x	y	z
C13	0.5164	0.4587	0.2959
C23	0.4802	0.3192	0.2005
C33	0.5497	0.3684	0.0677
C43	0.4847	0.5270	0.0256
C53	0.5219	0.6575	0.1286
C63	0.4474	0.8138	0.0961
O23	0.5548	0.1810	0.2467
O33	0.4966	0.2429	-0.0230
O43	0.5683	0.5854	-0.0899
O53	0.4481	0.6008	0.2491
O63	0.5448	0.9045	-0.0010
H13	0.6557	0.4850	0.3086
H23	0.3412	0.2845	0.1941

H33	0.6907	0.3840	0.0706
H43	0.3458	0.5046	0.0087
H53	0.6613	0.6859	0.1397
H63A	0.3136	0.7854	0.0645
H63B	0.4413	0.8877	0.1838
C14	0.4836	0.5413	0.7959
C24	0.5198	0.6808	0.7005
C34	0.4503	0.6316	0.5677
C44	0.5153	0.4730	0.5256

Table A (cont.)

C54	0.4781	0.3425	0.6286
C64	0.5526	0.1862	0.5961
O24	0.4452	0.8190	0.7467
O34	0.5034	0.7571	0.4770
O44	0.4317	0.4146	0.4101
O54	0.5519	0.3992	0.7491
O64	0.4552	0.0955	0.4990
H14	0.3443	0.5150	0.8086
H63O	0.1697	0.6400	0.3712
C14	0.4680	0.5220	-0.1500
C24	0.3180	0.5060	-0.0540
C34	0.3980	0.5590	0.0820
O24	0.2300	0.6030	-0.0920
C44	0.5090	0.4680	0.1190
O34	0.2500	0.5230	0.1700
C54	0.6400	0.4740	0.0110
O14	0.6210	0.5390	0.2320
O54	0.5410	0.4130	-0.1080
C64	0.7570	0.3920	0.0370
O64	0.8860	0.4180	-0.0670
H14	0.5652	0.6374	-0.1577
H24	0.2243	0.3886	-0.0506
H34	0.4800	0.6792	0.0821
H44	0.4232	0.3516	0.1370
H54	0.7246	0.5920	-0.0036
H64A	0.8256	0.4356	0.1166
H64B	0.6794	0.2739	0.0479
H24O	0.2397	0.6679	-0.0333
H34O	0.2909	0.5499	0.2434
H64O	0.8303	0.3600	-0.1288

[a)] Atoms assigned the label 2 and 4 are symmetry related to the ones with label 1 and 3 by a 2_1 screw axis, respectively

Table B.

Fractional coordinates of mercerized cellulose II . Monoclinic unit cell, space group $P2_1$: a = 8.10 Å, b = 9.03 Å, c(fiber axis) = 10.31 Å, γ = 117.1°. Antiparallel chains.

Chain 1 (corner)

Atoms [a)]	x	y	z
C11	-0.0430	0.0070	0.3810
C21	-0.1250	0.0860	0.2860
C31	-0.1510	-0.0030	0.1560
O21	-0.2990	0.0620	0.3340
C41	0.0340	0.0080	0.1120
O31	-0.2240	0.0690	0.0660
C51	0.1180	-0.0570	0.2160
O11	0.0110	-0.0910	-0.0010
O51	0.1330	0.0340	0.3330
C61	0.2980	-0.0530	0.1830
O61	0.3370	-0.1550	0.2700
H11	-0.1257	-0.1115	0.3924
H21	-0.0411	0.2049	0.2764
H31	-0.2396	-0.1205	0.1677
H41	0.1198	0.1243	0.0929

H51	0.0297	-0.1731	0.2320
H61A	0.2935	-0.0928	0.0947
H61B	0.3960	0.0603	0.1874
H21O	-0.3801	0.0096	0.2806
H31O	-0.2428	0.0189	-0.0036
H61O	0.3446	-0.1196	0.3443
C12	0.0430	-0.0070	0.8810
C22	0.1250	-0.0860	0.7860
C32	0.1510	0.0030	0.6560
O22	0.2990	-0.0620	0.8340
C42	-0.0340	-0.0080	0.6120
O32	0.2240	-0.0690	0.5660
C52	-0.1180	0.0570	0.7160
O12	-0.0110	0.0910	0.4990
O52	-0.1330	-0.0340	0.8330
C62	-0.2980	0.0530	0.6830
O62	-0.3370	0.1550	0.7700
H12	0.1257	0.1115	0.8924
H22	0.0411	-0.2049	0.7764

Table B (cont.)

H32	0.2396	0.1205	0.6677
H42	-0.1198	-0.1243	0.5929
H52	-0.0297	0.1731	0.7320
H62A	-0.2935	0.0928	0.5947
H62B	-0.3960	-0.0603	0.6874
H22O	0.3801	-0.0096	0.7806
H32O	0.2428	-0.0189	0.4964
H62O	-0.3446	0.1196	0.8443

Chain 2 (center):

Atoms	x	y	z
C13	0.5320	0.4780	0.3500
C23	0.6820	0.4940	0.4460
C33	0.6020	0.4410	0.5820
O23	0.7700	0.3970	0.4080
C43	0.4910	0.5320	0.6190
O33	0.7500	0.4770	0.6700
C53	0.3600	0.5260	0.5110
O13	0.3790	0.4610	0.7320
O53	0.4590	0.5870	0.3920
C63	0.2430	0.6080	0.5370
O63	0.1140	0.5820	0.4330
H13	0.4348	0.3626	0.3423
H23	0.7757	0.6114	0.4494
H33	0.5200	0.3208	0.5821
H43	0.5768	0.6484	0.6370
H53	0.2754	0.4080	0.4964
H63A	0.1744	0.5644	0.6166
H63B	0.3206	0.7261	0.5479
H23O	0.7603	0.3321	0.4667
H33O	0.7091	0.4501	0.7434
H63O	0.1697	0.6400	0.3712
C14	0.4680	0.5220	-0.1500
C24	0.3180	0.5060	-0.0540
C34	0.3980	0.5590	0.0820
O24	0.2300	0.6030	-0.0920
C44	0.5090	0.4680	0.1190
O34	0.2500	0.5230	0.1700
C54	0.6400	0.4740	0.0110
O14	0.6210	0.5390	0.2320
O54	0.5410	0.4130	-0.1080
C64	0.7570	0.3920	0.0370
O64	0.8860	0.4180	-0.0670
H14	0.5652	0.6374	-0.1577
H24	0.2243	0.3886	-0.0506
H34	0.4800	0.6792	0.0821
H44	0.4232	0.3516	0.1370
H54	0.7246	0.5920	-0.0036
H64A	0.8256	0.4356	0.1166

H64B	0.6794	0.2739	0.0479
H24O	0.2397	0.6679	-0.0333
H34O	0.2909	0.5499	0.2434
H64O	0.8303	0.3600	-0.1288

[a)] Atoms assigned the label 2 and 4 are symmetry related to the ones with label 1 and 3 by a 2_1 screw axis, respectively.

Table C
Fractional coordinates of cellulose III_1. Monoclinic unit cell, space group close to P 2_1: a= 10.25 Å, b = 7.78 Å, c(fiber axis) = 10.34 Å, γ = 122.4^o . Parallel chains.

Chain 1 (corner):

Atoms	x	y	z
O41	-0.0515	-0.1312	0.0000
C41	0.0201	-0.0125	0.1125
C11	-0.0106	0.0339	0.3832
C31	-0.0698	0.0794	0.1589
C21	-0.0083	0.1842	0.2879
C51	0.0202	-0.1510	0.2163
O51	0.0808	-0.0399	0.3344
O21	-0.1004	0.2565	0.3357
O31	-0.0601	0.2212	0.0656
C61	0.1172	-0.2384	0.1832
O61	0.0551	-0.3748	0.0752
H11	-0.1248	-0.0884	0.3972

Table C (cont.)

H21	0.1058	0.3078	0.2761
H31	-0.1863	-0.0377	0.1701
H41	0.1343	0.1039	0.0910
H51	-0.0941	-0.2717	0.2324
H61A	0.1235	-0.3155	0.2638
H61B	0.2292	-0.1180	0.1597
H21O	-0.0362	0.3801	0.3903
H31O	-0.1482	0.1507	0.0035
H61O	0.0391	-0.5094	0.0991
O42	0.0515	0.1312	0.5000
C42	-0.0215	0.0150	0.6131
C12	0.0111	-0.0361	0.8827
C32	0.0605	-0.0891	0.6569
C22	-0.0016	-0.1920	0.7863
C52	-0.0117	0.1586	0.7179
O52	-0.0734	0.0492	0.8364
O22	0.0838	-0.2758	0.8316
O32	0.0414	-0.2352	0.5627
C62	-0.1003	0.2586	0.6874
O62	-0.0400	0.3871	0.5757
H12	0.1276	0.0795	0.8953
H22	-0.1181	-0.3089	0.7759
H32	0.1790	0.0211	0.6666
H42	-0.1378	-0.0949	0.5930
H52	0.1049	0.2727	0.7325
H62A	-0.0960	0.3449	0.7673
H62B	-0.2162	0.1444	0.6697
H22O	0.0118	-0.4151	0.8677
H32O	0.1411	-0.1854	0.5163
H62O	-0.0017	0.5309	0.5999

Chain 2 (center):

Atoms	x	y	z
O43	0.4563	0.3692	-0.0870
C43	0.5241	0.4875	0.0263
C13	0.4840	0.5328	0.2953
C33	0.4325	0.5791	0.0687
C23	0.4896	0.6835	0.1984
C53	0.5207	0.3487	0.1317

O53	0.5771	0.4593	0.2504
O23	0.3959	0.7556	0.2423
O33	0.4456	0.7213	-0.0259
C63	0.6185	0.2613	0.1027
O63	0.5531	0.1125	0.0017
H13	0.3694	0.4105	0.3071
H23	0.6042	0.8071	0.1889
H33	0.3158	0.4620	0.0775
H43	0.6389	0.6040	0.0072
H53	0.4058	0.2279	0.1455
H63A	0.6302	0.1950	0.1868
H63B	0.7288	0.3804	0.0736
H23O	0.4528	0.8645	0.3085
H33O	0.3529	0.6552	-0.0838
H63O	0.5781	0.0062	0.0164
O44	0.5420	0.6297	0.4130
C44	0.4750	0.5104	0.5260
C14	0.5142	0.4671	0.7956
C34	0.5702	0.4245	0.5696
C24	0.5135	0.3193	0.6990
C54	0.4736	0.6463	0.6310
O54	0.4179	0.5350	0.7495
O24	0.6104	0.2529	0.7441
O34	0.5618	0.2848	0.4753
C64	0.3718	0.7274	0.6008
O64	0.4397	0.8848	0.5050
H14	0.6274	0.5924	0.8080
H24	0.4003	0.1928	0.6889
H34	0.6859	0.5449	0.5792
H44	0.3614	0.3908	0.5062
H54	0.5872	0.7702	0.6455
H64A	0.3521	0.7841	0.6857
H64B	0.2654	0.6073	0.5658
H24O	0.5528	0.1383	0.8068
H34O	0.6463	0.3587	0.4102
H64O	0.4090	0.9853	0.5211

Table D
Fractional coordinates of cellulose IV_1 . Unit cell:, a = 8.03 Å, b = 8.13 Å, c(fiber axis) = 10.34 Å, $\alpha = \beta = \gamma = 90.0^{o}$.
Space group P 1. Dimer as basic building unit. Parallel chains

Chain 1 (corner):

Atoms	x	y	z
C11	-0.0054	0.0418	0.3787
C21	0.0232	0.1818	0.2837
C31	-0.0484	0.1364	0.1531
C41	0.0161	-0.0294	0.1085
C51	-0.0091	-0.1592	0.2128
C61	0.0670	-0.3230	0.1771
O21	-0.0514	0.3282	0.3313
O31	-0.0072	0.2585	0.0590
O41	-0.0704	-0.0801	-0.0045
O51	0.0679	-0.1059	0.3304
O61	-0.0397	-0.4129	0.0912
H11	-0.1335	0.0244	0.3932
H21	0.1518	0.2011	0.2737
H31	-0.1787	0.1299	0.1611
H41	0.1436	-0.0196	0.0875
H51	-0.1372	-0.1750	0.2287
H61A	0.0875	-0.3923	0.2612
H61B	0.1816	-0.3023	0.1309
C12	0.0065	-0.0434	0.8789
C22	-0.0225	-0.1835	0.7834
C32	0.0498	-0.1384	0.6531
C42	-0.0152	0.0274	0.6082
C52	0.0101	0.1576	0.7129

C62	-0.0661	0.3216	0.6775
O22	0.0514	-0.3304	0.8310
O32	0.0092	-0.2605	0.5588
O42	0.0715	0.0782	0.4954
O52	-0.0671	0.1043	0.8306
O62	0.0582	0.4322	0.6292
H12	0.1347	-0.0261	0.8932
H22	-0.1513	-0.2022	0.7731
H32	0.1800	-0.1315	0.6616
H42	-0.1427	0.0175	0.5871
H52	0.1382	0.1734	0.7289
H62A	-0.1232	0.3733	0.7593
H62B	-0.1567	0.3032	0.6056
Chain 2 (center):			
C13	0.4998	0.5422	0.1017
C23	0.5453	0.6776	-0.0067
C33	0.4686	0.6413	-0.1239
C43	0.5121	0.4689	-0.1685
C53	0.4710	0.3432	-0.0642
C63	0.5263	0.1715	-0.0999
O23	0.4895	0.8320	0.0544
O33	0.5247	0.7576	-0.2180
O43	0.4200	0.4290	-0.2815
O53	0.5540	0.3867	0.0534
O63	0.4177	0.1010	-0.1950
H13	0.3702	0.5405	0.1162
H23	0.6755	0.6812	-0.0033
H33	0.3390	0.6514	-0.1133
H43	0.6400	0.4632	-0.1895
H53	0.3418	0.3431	-0.0483
H63A	0.5269	0.0970	-0.0168
H63B	0.6474	0.1769	-0.1378
C14	0.5009	0.4562	0.6019
C24	0.4547	0.3207	0.5064
C34	0.5321	0.3567	0.3761
C44	0.4882	0.5292	0.3312
C54	0.5294	0.6552	0.4359
C64	0.4740	0.8273	0.4005
O24	0.5098	0.1659	0.5541
O34	0.4767	0.2403	0.2818
O44	0.5804	0.5691	0.2184
O54	0.4461	0.6117	0.5536
O64	0.6146	0.9342	0.3860
H14	0.6303	0.4579	0.6163
H24	0.3247	0.3177	0.4962
H34	0.6620	0.3477	0.3846
H44	0.3604	0.5347	0.3103
H54	0.6584	0.6555	0.4519
H64A	0.3951	0.8733	0.4730
Table d (cont)			
H64B	0.4083	0.8230	0.3128

Table E
Fractional coordinates of cellulose IV_2. Unit cell: a = 7.99 Å, b = 8.10 Å, c(fiber axis) = 10.34 Å, $\alpha = \beta = \gamma = 90.0^{o}$
Space group P 1. Dimer as basic building unit. Antiparallel chains.

Chain 1 (corner):			
Atoms	x	y	z
C11	0.0075	-0.0435	0.4311
C21	-0.0185	-0.1840	0.3356
C31	0.0542	-0.1360	0.2059
C41	-0.0158	0.0281	0.1607
C51	0.0074	0.1590	0.2657

C61	-0.0717	0.3227	0.2309
O21	0.0594	-0.3296	0.3832
O31	0.0194	-0.2595	0.1109
O41	0.0697	0.0812	0.0477
O51	-0.0681	0.1044	0.3838
O61	0.0522	0.4379	0.1870
H11	0.1363	-0.0238	0.4443
H21	-0.1474	-0.2057	0.3250
H31	0.1845	-0.1248	0.2156
H41	-0.1437	0.0151	0.1401
H51	0.1359	0.1770	0.2813
H61A	-0.1333	0.3711	0.3122
H61B	-0.1596	0.3038	0.1569
C12	-0.0064	0.0426	0.9311
C22	0.0196	0.1830	0.8356
C32	-0.0531	0.1351	0.7056
C42	0.0169	-0.0291	0.6607
C52	-0.0061	-0.1601	0.7657
C62	0.0728	-0.3236	0.7309
O22	-0.0581	0.3286	0.8832
O32	-0.0181	0.2585	0.6109
O42	-0.0640	-0.0859	0.5477
O52	0.0693	-0.1054	0.8838
O62	-0.0274	-0.4107	0.6384
H12	-0.1350	0.0230	0.9457
H22	0.1486	0.2044	0.8250
H32	-0.1835	0.1240	0.7152
H42	0.1452	-0.0154	0.6416
H52	-0.1348	-0.1769	0.7813
H62A	0.0861	-0.3957	0.8147
H62B	0.1916	-0.3020	0.6911

Chain 2 (center):

Atoms	x	y	z
C13	0.4959	0.4574	0.7230
C23	0.5297	0.3186	0.8186
C33	0.4544	0.3626	0.9485
C43	0.5153	0.5304	0.9934
C53	0.4850	0.6599	0.8885
C63	0.5549	0.8273	0.9232
O23	0.4601	0.1690	0.7710
O33	0.4960	0.2412	1.0432
O43	0.4314	0.5827	1.1065
O53	0.5633	0.6093	0.7704
O63	0.4641	0.8989	1.0287
H13	0.3665	0.4699	0.7084
H23	0.6596	0.3041	0.8291
H33	0.3237	0.3668	0.9390
H43	0.6442	0.5235	1.0126
H53	0.3557	0.6710	0.8728
H63A	0.5479	0.9057	0.8425
H63B	0.6809	0.8140	0.9502
C14	0.5051	0.5441	0.2230
C24	0.4713	0.6831	0.3186
C34	0.5467	0.6390	0.4483
C44	0.4859	0.4714	0.4934
C54	0.5161	0.3420	0.3885
C64	0.4461	0.1743	0.4232
O24	0.5412	0.8326	0.2710
O34	0.5051	0.7605	0.5432

Table E (cont)

O44	0.5741	0.4230	0.6065
O54	0.4377	0.3923	0.2704
O64	0.5776	0.0547	0.4357
H14	0.6348	0.5314	0.2099
H24	0.3416	0.6978	0.3291
H34	0.6773	0.6348	0.4386
H44	0.3573	0.4777	0.5140
H54	0.6905	0.3309	0.3728

H64A	0.3618	0.1360	0.3513
H64B	0.3821	0.1832	0.5116